NASA TECHNICAL NOTE

NASA TN D-4495

A BREADBOARD FLUERIC-CONTROLLED PNEUMATIC STEPPING-MOTOR SYSTEM

by William S. Griffin

Lewis Research Center
Cleveland, Ohio

NATIONAL AERONAUTICS AND SPACE ADMINISTRATION • WASHINGTON, D. C. • APRIL 1968

A BREADBOARD FLUERIC-CONTROLLED PNEUMATIC STEPPING-MOTOR SYSTEM

By William S. Griffin

Lewis Research Center
Cleveland, Ohio

NATIONAL AERONAUTICS AND SPACE ADMINISTRATION

For sale by the Clearinghouse for Federal Scientific and Technical Information
Springfield, Virginia 22151 – CFSTI price $3.00

A BREADBOARD FLUERIC-CONTROLLED PNEUMATIC STEPPING-MOTOR SYSTEM

by William S. Griffin

Lewis Research Center

SUMMARY

This report describes NASA Lewis developed flueric[1] circuitry used to drive a novel pneumatic stepping motor. The design and breadboard implementation of the circuitry are presented along with some of the techniques used for interconnection of digital fluid jet amplifiers. The experimental performance of a breadboard flueric-drive-circuitry - stepping-motor actuator system is evaluated. Finally, a comparison is made between the resultant pneumatic stepping-motor system and the more conventional pneumatic piston-in-cylinder actuator.

The principal conclusions of the work are that

(1) The NASA flueric-drive-circuitry - stepping-motor combination constitutes a reliable, fast, open-loop digital stepping actuator system which has high resolution and output stiffness. The breadboard flueric-drive-circuitry - stepping-motor system could be stepped at 173 steps per second in either direction and cyclicly reversed, without missing steps, at 115 steps per second. The step size of the shaft output motion was 0.25^{o} and a maximum static output torque of 70 inch-pounds force (788.9 cm-N) was obtained.

(2) The flueric-drive-circuitry - stepping-motor actuator system consumes more flow than a conventional electropneumatic piston-in-cylinder actuator designed to do the same job.

INTRODUCTION

The advent of the nuclear engine for rocket vehicle application (NERVA) created a demand for actuator systems which are simple and reliable, have a minimum of moving

[1]Fluerics is the term adopted in July 1965 by the Government Fluid Amplifier Coordination Group to describe a general class of fluid devices, such as fluid jet amplifiers, vortex amplifiers, turbulence amplifiers, etc. Fluerics is used throughout this report to denote such devices.

parts and sliding surfaces, and can withstand a high surrounding nuclear radiation field. As a result of these requirements, a novel pneumatic stepping motor was developed by the Bendix Corporation under NASA contract NAS 3-5214. The motor, which operates on the nutating gear principle, can be operated either digitally or in analog fashion. Development of a complete actuator system, however, required synthesis of means for admitting the various working pressures to the stepping motor. Preferably, the devices for introducing working pressures should be simple and at least as reliable as the stepping motor itself. Because of the radiation level at the actuator location, the advantages of fluid amplifiers for this purpose appeared obvious.

Several approaches have been taken to develop a fluid-amplifier drive circuit for the stepping motor. Under NASA contract NAS 3-5214, an analog circuit composed of vortex amplifiers was developed. Although this circuit had the advantage of being proportional, thus enabling the motor to be reverse driven under excessive load torques, it proved much slower than specified (ref. 1). An alternative method for driving the motor was proposed by Blaiklock (ref. 2). Blaiklock's circuit is digital and open loop in design and uses fluid jet amplifiers rather than vortex amplifiers. Thus, it is expected to be faster than the analog circuit of reference 1. However, Blaiklock's circuit requires successful development of an axisymmetric, tristable fluid jet amplifier for its successful implementation.

The approach described in this report was to design and develop a high-speed, open-loop, digital stepping circuit which could be easily synthesized from fluid jet amplifiers of conventional design. The design and breadboard implementation of this stepping-motor drive circuitry (ref. 3), its performance, and the performance of the complete drive-circuitry - stepping-motor actuator system are described herein. The nomenclature, some of the techniques used for interconnection of the elements, and details of the design of certain subassemblies are presented in appendixes A to C. Finally, a comparison is made between the flueric-drive-circuitry - stepping-motor actuator system and the more conventional pneumatic piston-in-cylinder actuator.

STEPPING MOTOR

As shown schematically in figure 1, the actuator has only two moving parts: a gimbal-supported driving gear free to nutate (wobble) but not to rotate and an output gear free to rotate but not to nutate. By unequal pressurization of eight bellows attached to its periphery, the driving gear is made to tilt and contact the output gear. As the bellows pressurization pattern is sequenced, the point of contact between the two gears travels around the circumference of the output gear. Since the output gear has 180 teeth and the nutating gear 181, the output gear advances by 1 tooth, or 2^{o}, for every complete revolu-

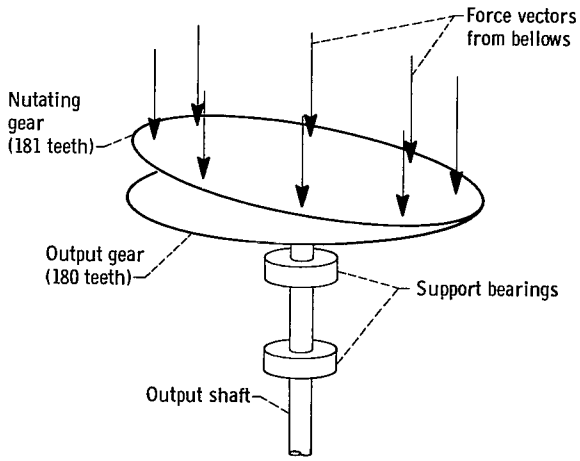

Figure 1. - Stepping-motor operation.

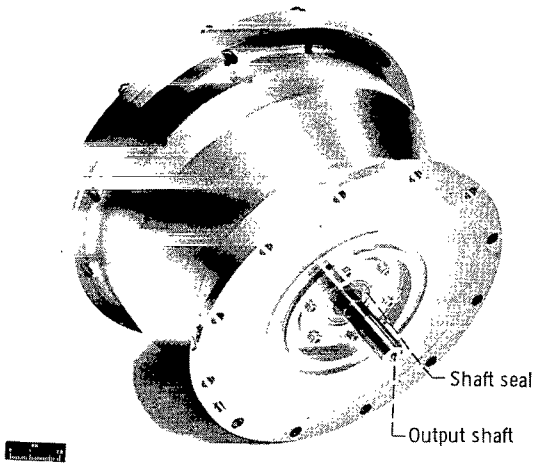

C-66-3984

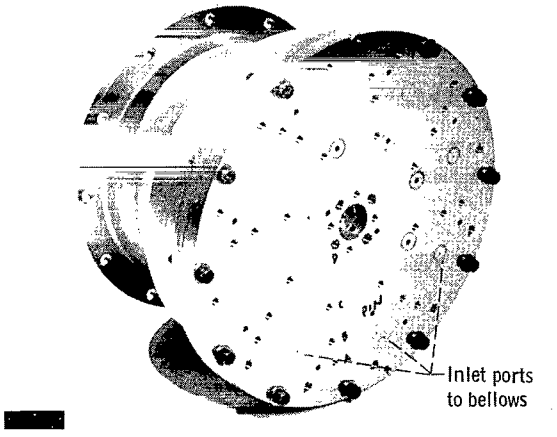

C-66-3983

Figure 2. - Stepping motor.

tion made by the point of contact. If the bellows pressurization pattern, and hence the point of contact, is advanced only by a fraction of a revolution, the output shaft will be advanced by the same fraction of 2^{o}. Since eight bellows are used for manipulation of the driving gear, the pressurization pattern can be cyclicly advanced in eight steps and the output-shaft position in increments of 0.25^{o}. If the bellows pressurization pattern is fixed at one position, the output-shaft position is also fixed for any load torques less than those which would cause disengagement of the gears. When load torques are applied, a small output-shaft deflection occurs accompanied by movement of the nutating gear. However, for torques less than those which cause disengagement, the maximum output-shaft deflection is less than one step size (0.25^{o}). Thus, in the absence of excessive load torques, the actuator motor can accurately position a load at any shaft position specified by sequencing of the bellows pressurization pattern.

The motor and its cross-sectional drawing are shown in figures 2 and 3, respectively. A more complete description of the motor and the procedures used in its design is given in reference 1.

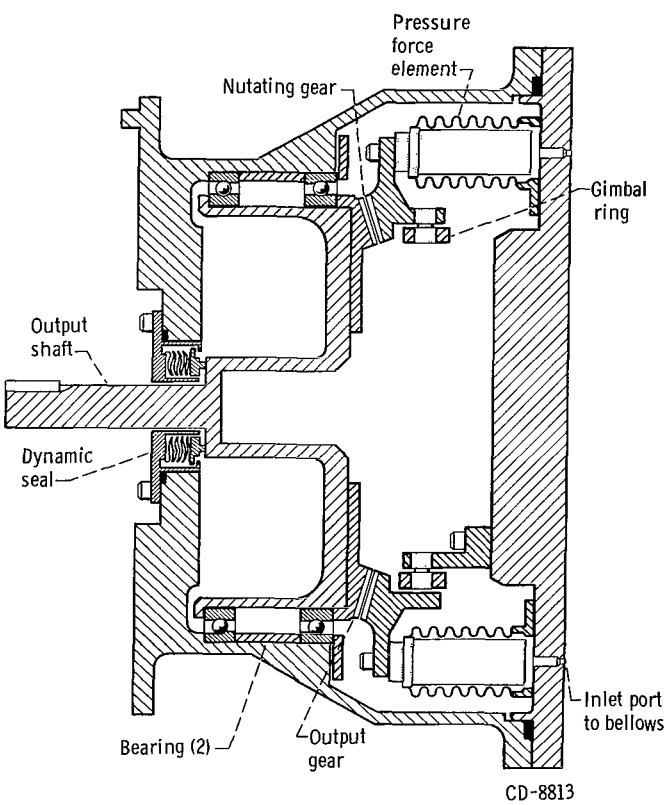

Figure 3. - Cross section of pneumatic stepping motor.

BELLOWS DRIVE CIRCUITRY DESIGN

A key performance requirement affecting the design of the bellows drive circuit was that it sequence the bellows pressures in excess of 160 steps per second. An open-loop digital counting circuit was used to achieve this sequencing speed. With no external position feedback, the circuit speed of operation was limited only by the speed of its elements and the delays of its internal logic feedback paths. Fluid jet amplifiers were used as the operational elements since they tend to be of the order of 3 to 10 times faster than other flueric components (vortex amplifiers, turbulence amplifiers, or impact modulators).

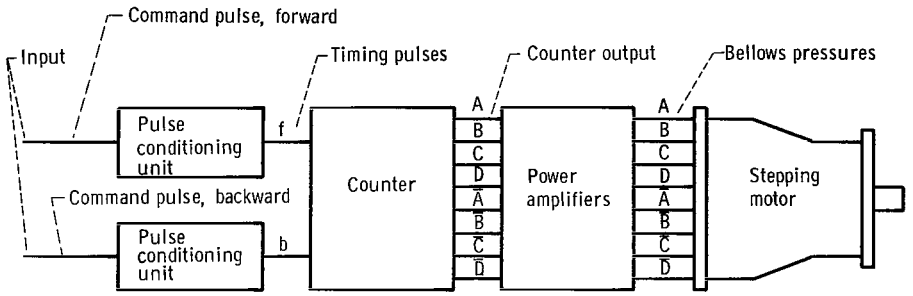

Figure 4. - Block diagram of breadboard actuator system.

Figure 4 is a block diagram of the drive-circuitry and stepping-motor actuation system. The drive circuitry consists of three main parts: (1) two pulse conditioning units which accept forward and backward directing command pulses and convert them into well-defined timing pulses T_f and T_b, (2) a counter circuit which accepts the timing pulses and uses them to advance a pressurization pattern on its eight outputs, and (3) the power amplifiers which take the low-power signals delivered by the counter and convert them into high pressure and flow signals for driving the bellows of the stepping motor. The following sections discuss design aspects of the various circuit components.

Counting Circuit

The counting circuit is a ring-type counter on which is stored a pressurization pattern shifted forward or backward by either of two timing pulse trains. As shown schematically by the darkened circles in figure 5(a), the required pressurization pattern groups four pressurized bellows next to each other so that maximum force is exerted on the point of contact between the nutating and output gears. To be avoided is a pressurization pattern, such as that shown in figure 5(b), which shifts the center of

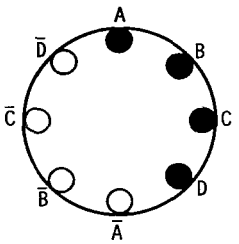

(a) Correct pressurization pattern.

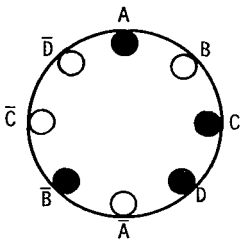

(b) Incorrect pressurization pattern.

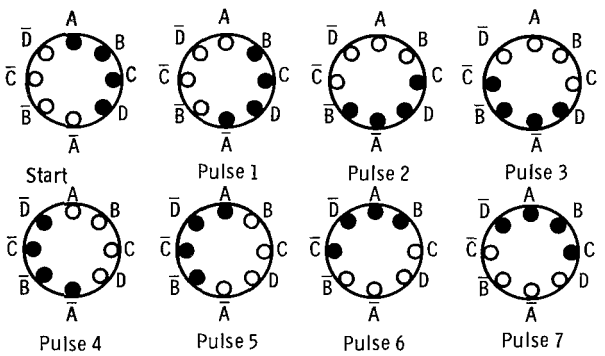

(c) Sequencing of pressure pattern by forward counting input pulses.

Figure 5. - Bellows pressurization patterns.

TABLE I. - SEQUENCING OF PRESSURIZATION PATTERN

Forward timing pulse, T_f	Backward timing pulse, T_b	Bellows							
		A	B	C	D	$\bar{A}$	$\bar{B}$	$\bar{C}$	$\bar{D}$
0	0	1	1	1	1	0	0	0	0
1	0	0	1	1	1	1	0	0	0
2	0	0	0	1	1	1	1	0	0
3	0	0	0	0	1	1	1	1	0
4	0	0	0	0	0	1	1	1	1
5	0	1	0	0	0	0	1	1	1
6	0	1	1	0	0	0	0	1	1
7	0	1	1	1	0	0	0	0	1
8	0	1	1	1	1	0	0	0	0
0	0	1	1	1	1	0	0	0	0
0	1	1	1	1	0	0	0	0	1
0	2	1	1	0	0	0	0	1	1
0	3	1	0	0	0	0	1	1	1
0	4	0	0	0	0	1	1	1	1
0	5	0	0	0	1	1	1	1	0
0	6	0	0	1	1	1	1	0	0
0	7	0	1	1	1	1	0	0	0
0	8	1	1	1	1	0	0	0	0

force toward the center of the nutating gear and delivers a higher percentage of the bellows output force to the gimbals which support the nutating gear rather than to the point of contact between the gears. Thus, the counting circuit is required to maintain the pressurization pattern shown in figure 5(a) and to index this pattern sequentially around the circumference of the nutating gear, as shown in figure 5(c).

If bellows pressurization is denoted by the logical state 1 and absence of bellows pressurization by the logical state 0, then the following set of logical equations may be used to represent the sequencing of the pressurization pattern:

$$\left.\begin{aligned}
S_A &= T_b \cdot B + T_f \cdot \overline{D} + B \cdot \overline{D} = R_{\overline{A}} \\
R_A &= T_b \cdot \overline{B} + T_f \cdot D + \overline{B} \cdot D = S_{\overline{A}} \\
S_B &= T_b \cdot C + T_f \cdot A = R_{\overline{B}} \\
R_B &= T_b \cdot \overline{C} + T_f \cdot \overline{A} = S_{\overline{B}} \\
S_C &= T_b \cdot D + T_f \cdot B + B \cdot D = R_{\overline{C}} \\
R_C &= T_b \cdot \overline{D} + T_f \cdot \overline{B} + \overline{B} \cdot \overline{D} = S_{\overline{C}} \\
S_D &= T_b \cdot \overline{A} + T_f \cdot C = R_{\overline{D}} \\
R_D &= T_b \cdot A + T_f \cdot \overline{C} = S_{\overline{D}}
\end{aligned}\right\} \qquad (1)$$

Setting A (S_A) denotes transition of bellows A from logical state 0 to logical state 1 while resetting A (R_A) denotes transition from 1 to 0. Because of the symmetry of the pressurization pattern, $S_A \longleftrightarrow R_{\overline{A}}$ while $S_{\overline{A}} \longleftrightarrow R_A$. The symbols $\cdot$ and $+$ denote logical AND and logical OR, respectively. Table I represents, in tabular form, the sequencing of the bellows pressures as a function of forward or backward timing pulses.

Two comments should be made regarding logical equations (1). First, the equations were derived by using a synthesis procedure described in reference 4, and make use of the fact that only eight of the possible combinations of the four Boolean variables A, B, C, and D represent acceptable pressurization patterns. The resultant Set and Reset equations (minus the error correcting terms) contain a minimum number of terms. These equations enable the use of a simple circuit design which has low flow consumption. During application of the timing pulses, four Set and Reset equations are satisfied by any given counter state. However, three of these are redundant and simply instruct a bistable element to remain in the state it is already in. As long as a correct

pressurization pattern has been initially stored on the counter, this redundancy does not affect the desired counting sequence, and no need exists for error correction.

Secondly, four terms in the logical equations do not contain either forward T_f or backward T_b pulses. These terms are error correcting terms, which detect an incorrect pressurization pattern, such as shown in figure 5(b), and issue the appropriate Set or Reset signal to eliminate it. Without these terms, an incorrect pressurization pattern would remain incorrect as it was propagated around the outputs of the counter. At times, the error correcting terms issue a signal when an error does not exist. However, the generation of an additional signal under normal operation is again a redundancy which instructs the affected fluid jet amplifier to remain in the state it is already in. Thus, the error-correcting term for S_C would issue a Set signal for C during the initial state of the counter in table I even though no error was present. Once the counter had been advanced two steps forward (from T_f - 0 to T_f - 2 in table I), B would be logical 0 and would cause the error correction term $B \cdot D$ in S_C to also be logical 0 (i.e., to vanish).

The counter circuit which was developed to satisfy the logical equations (eqs. (1)) is shown schematically in figure 6. The pressurization pattern is stored and advanced on four central bistable fluid jet amplifiers, designated I, II, III, and IV. Their outputs are designated A, $\overline{A}$, B, $\overline{B}$, C, $\overline{C}$, D, and $\overline{D}$, respectively, corresponding to similarly designated bellows in figure 5. An active two-input OR unit is connected to each control port and furnishes its control signals. To the input of each active OR unit is connected the output of an OR unit acting as a passive AND. These units accept the output of one of the central bistable units as a power supply and a forward T_f or backward T_b timing pulse as their control signal. Their output is thus the logical product (AND) of the outputs of the central bistable units and the timing pulse. For example, the input delivered to bistable amplifier I from the passive AND unit A_1 is a reset for I and is the logical product of the forward pulse T_f and the output of D (i.e., $T_f \cdot D$). Examination of equation (1) shows that this is indeed the condition by which A is reset by a forward pulse. Careful examination of the circuit shows that the logical equations (1) including the error correcting terms are satisfied. The connections which implement the latter are shown as dotted lines in figure 6.

Operation of the circuit is as follows: Short timing pulses of one type only (either T_f or T_b) are applied simultaneously to all control ports of the passive AND units. Those AND units whose power nozzles are pressurized by the outputs of the central bistable amplifiers (I, II, III, and IV) generate output signals of duration approximately equal to the length of the timing pulse. These output signals travel to the control ports of the active OR units and cause them in turn to generate short output pulses. These pulses switch the central bistable amplifiers. The outputs of the central bistable units are delayed an amount of time τ before they reach the nozzles of the passive AND units. Thus, if the timing pulse is short and has vanished before changes in outputs from the

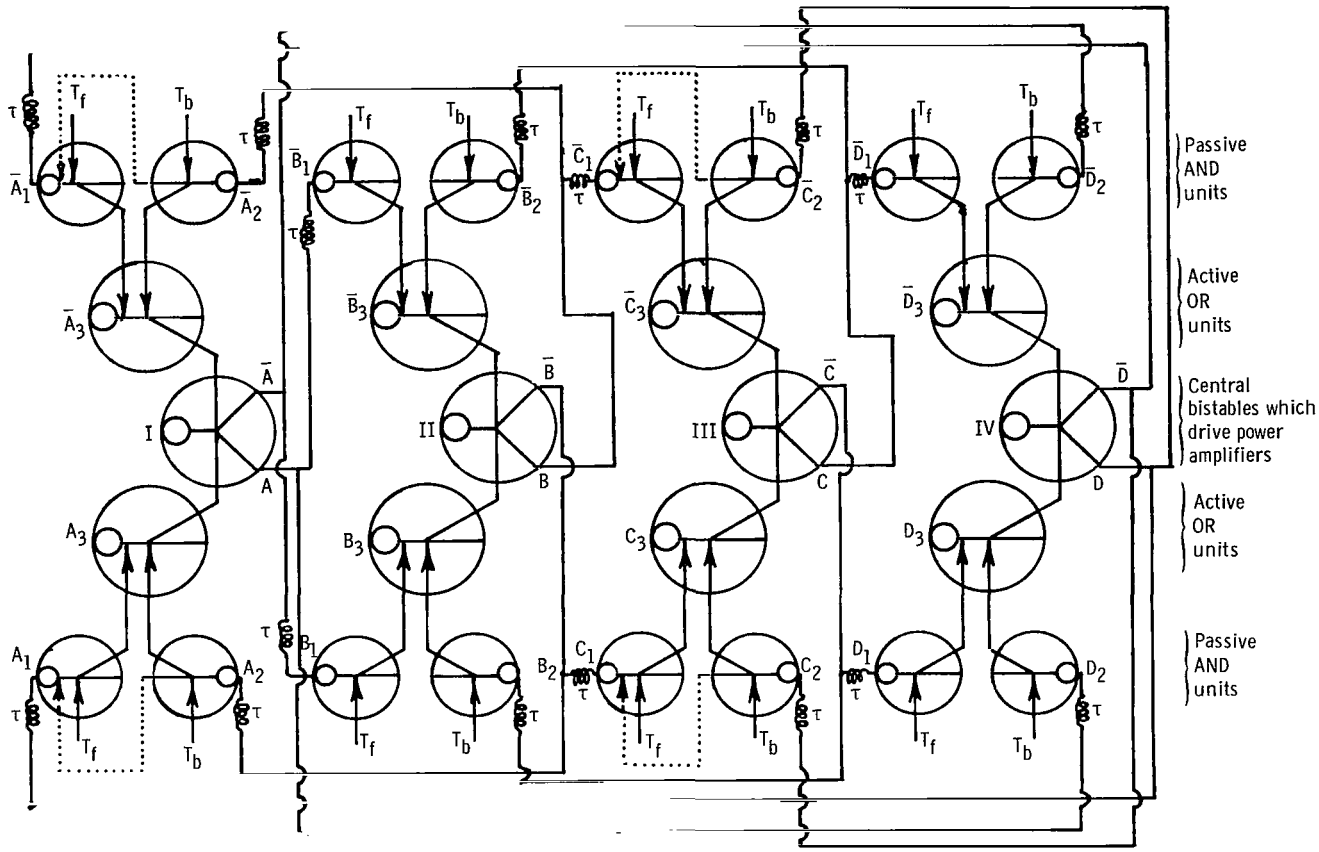

Figure 6. - Schematic diagram of counting circuit for nutator motor.

bistable amplifiers reach the power nozzles of the passive AND units, nothing further will happen and the counter will be set for the next timing pulse. The sequence is repeated with the application of each timing pulse T_f or T_b.

Choice of the proper delay τ with which to retard the carry signals from the central bistable units to the passive AND units is important. If the delay is too short, the carry signal will reach the power nozzles of the passive AND units before the timing pulse T_f has disappeared. If the delay is too long, the carry signals will not reach the power nozzles of the passive AND units by the time the next timing pulse occurs. Figure 7 schematically illustrates the time history of the various pressures in the counter circuit which are necessary to "set" A (i.e., cause the output A to appear).

If the counter is initially in the state T_f-3, as shown in table I, and if a forward timing pulse T_f is applied to the control ports of all the passive AND units, amplifier IV will be reset, and the output $\bar{D}$ will appear. The counter will thus have advanced to state T_f-4 of table I. Since the responses of the passive AND unit, the active OR unit, and the central bistable unit are not instantaneous, the output $\bar{D}$ will appear a time t_{sw}

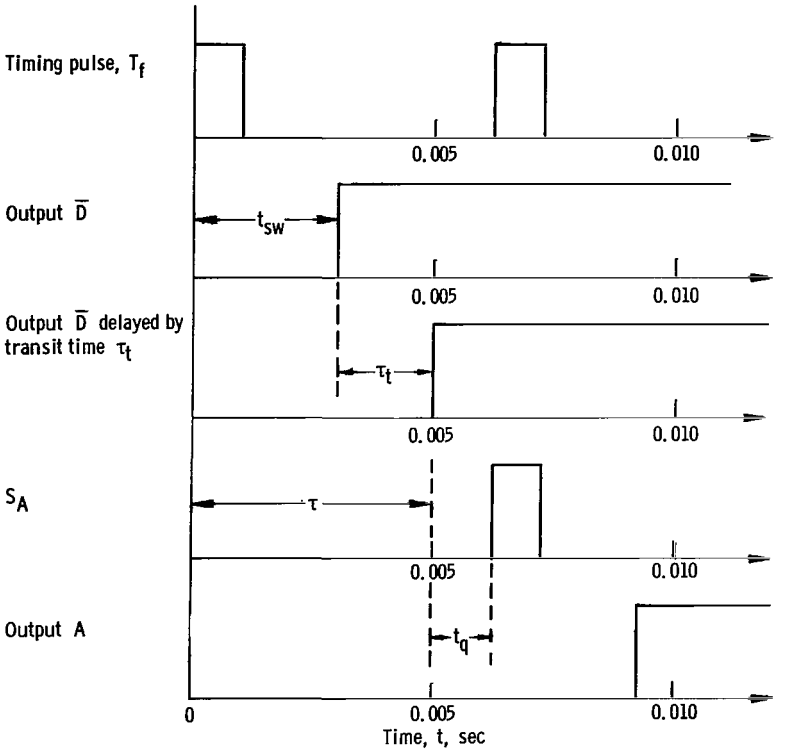

Figure 7. - Sequence of pressures necessary to set A.

after initiation of the timing pulse. The total switching time t_{sw}, pulse dispersion in the signal lines in the counter, and the rise and decay times of the timing pulse determine whether it is necessary to delay the carry signal by an additional amount of time τ_t to ensure that the timing signal has time to vanish. These times $\tau_t + t_{sw}$ constitute the total delay time τ, as is shown in figure 6. The resultant delayed output $\overline{D}_{delayed}$ is shown in the third line of figure 7 and sets the counter for the next timing pulse T_f. An amount of time t_q which exists between the last change of the carry signal $\overline{D}_{delayed}$ and the earliest possible occurrence of the next timing pulse T_f represents an idle counter state. A timing pulse may be again applied at any time during t_q to index the counter in its normal manner. Hence, the only inherent limit to the operating speed of the counter is the application of timing pulses so rapidly that the period t_q goes to zero. In the breadboard counter circuitry to be described in the section, BREADBOARD ACTUATOR SYSTEM, the width of the timing pulse was 1 millisecond, the total combined element switching time (including pulse propagation times within the elements) t_{sw} was approximately 0.0015 second, and the delay time τ_t was approximately 0.002 second. Since the actuator was designed to operate at 160 steps per second, the quiet period t_q is approximately 0.00275 second for the breadboard counter circuit which was implemented. Thus, the breadboard counter should be capable of operating at approximately

286 steps per second. If the measured delay in element switching time t_{sw} could be considered dependable, it could be used as the total delay time τ. With a total delay τ of only 0.0015 second, the circuit could, in theory, be stepped at 667 steps per second.

Pulse Conditioning Unit

As illustrated in figure 8(a), the command pulses delivered to the actuator system can be highly distorted as a result of propagating down a long transmission line. Their rounded leading edges, low amplitude, and long tails make them unsuitable for direct use as timing pulses. The function of the pulse conditioning unit, shown schematically in figure 8(b), is to convert the command pulses into properly shaped timing pulses.

The first element, an OR-NOR unit, is used to convert the command pulse, which is singlesided and of variable amplitude, into a push-pull signal of fixed amplitude. Since the output of the OR-NOR unit does not have fast rise and decay times, a bistable unit (unit 2 in fig. 8) is used to give the command pulse sharp leading and trailing edges. The

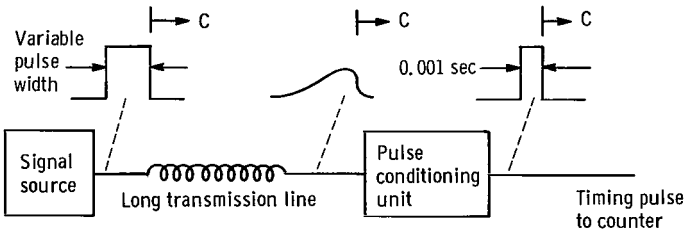

(a) Command pulse wave forms.

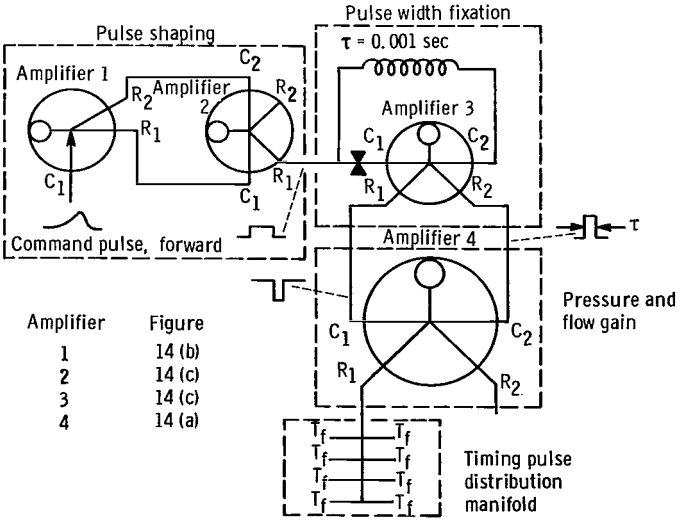

(b) Schematic diagram.

Figure 8. - Pulse conditioning unit.

output of unit 2 is fed into a unit which fixes the width of the pulse at 1 millisecond. This width was considered to be the minimum value compatible with the switching response of the passive AND units of the counter and the dispersive effects of the lines used to distribute the timing pulse. Pulse width fixation is accomplished by introducing the command pulse simultaneously to an orifice which feeds control port C_1 of amplifier 3 and to a 1-millisecond delay line connected to control port C_2 of the same amplifier. Thus, the reshaped command pulse initially causes flow to go through control port C_1 to set the amplifier, and to produce an output on receiver R_2. The same command pulse, however, propagates along the transmission line and, 1 millisecond later, pressurizes control port C_2. If the pulse delivered by the delay line is of proper magnitude, amplifier 3 will be reset and the flow from its receiver R_2 shut off, thus terminating the timing pulse. Design of the pulse width fixation portion is treated in appendix C. The remaining bistable amplifier, unit 4, serves to amplify the pulse in pressure and flow and send it to a manifold for distribution to the control ports of the passive AND units of the counter.

Power Amplifier

The Lewis SB1 power fluid jet amplifier was used to drive the bellows of the stepping motor. Shown in outline form in figure 9, the amplifier has a supersonic nozzle to create the main power jet and uses a conventional, inclined-wall interaction region for deflection of the jet. The receivers are of the Y type and follow the design philosophy used on the Lewis B1 subsonic bistable amplifier (ref. 5). Reverse discharge and displacement flows delivered by the bellows are thus dumped to atmosphere through the vent V_3 instead of into the interaction region. As pointed out in reference 5, this feature permits more rapid switching at lower control-port pressures and flows than would be

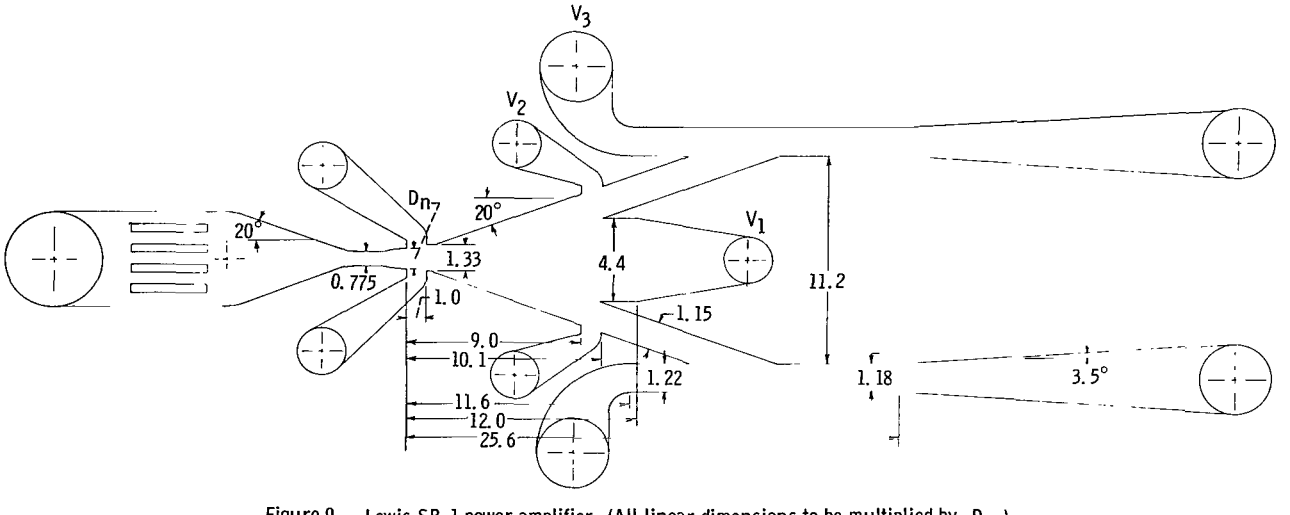

Figure 9. - Lewis SB-1 power amplifier. (All linear dimensions to be multiplied by D_n.)

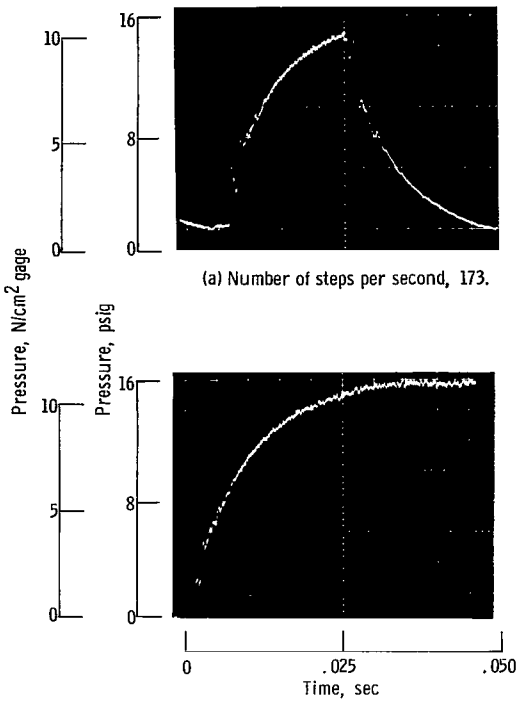

(a) Number of steps per second, 173.

(b) Number of steps per second, 28.7.

Figure 10. - Bellows pressure as function of time.

obtained with a fluid jet amplifier which used conventional receivers aimed at the interaction region. A penalty in pressure recovery associated with amplifiers using the Y type of receivers is believed to be offset by their increased switching speeds and lower control-port pressures.

The salient characteristics of the SB1 amplifier when driving the bellows are as follows:

Power nozzle throat size, in. (cm)	
Width	0.040 (0.101)
Depth	0.060 (0.153)
Design supply to exhaust pressure ratio	4.0
Maximum normalized receiver pressure (nominal), $(P_R - P_e)/(P_s - P_e)$, percent of supply	40
Maximum normalized receiver flow (nominal), $\dot{m}_R/\dot{m}_s$, percent of supply	80
Mach number of power nozzle	1.63
Design load volume, in.^{3} (cm^3)	0.576 (9.43)
Charging time constant of load volume, sec	0.008
Control-port switching pressure (nominal), $(P_c - P_e)/(P_s - P_e)$	0.07
Control-port switching flow (nominal), $\dot{m}_c/\dot{m}_s$	0.07

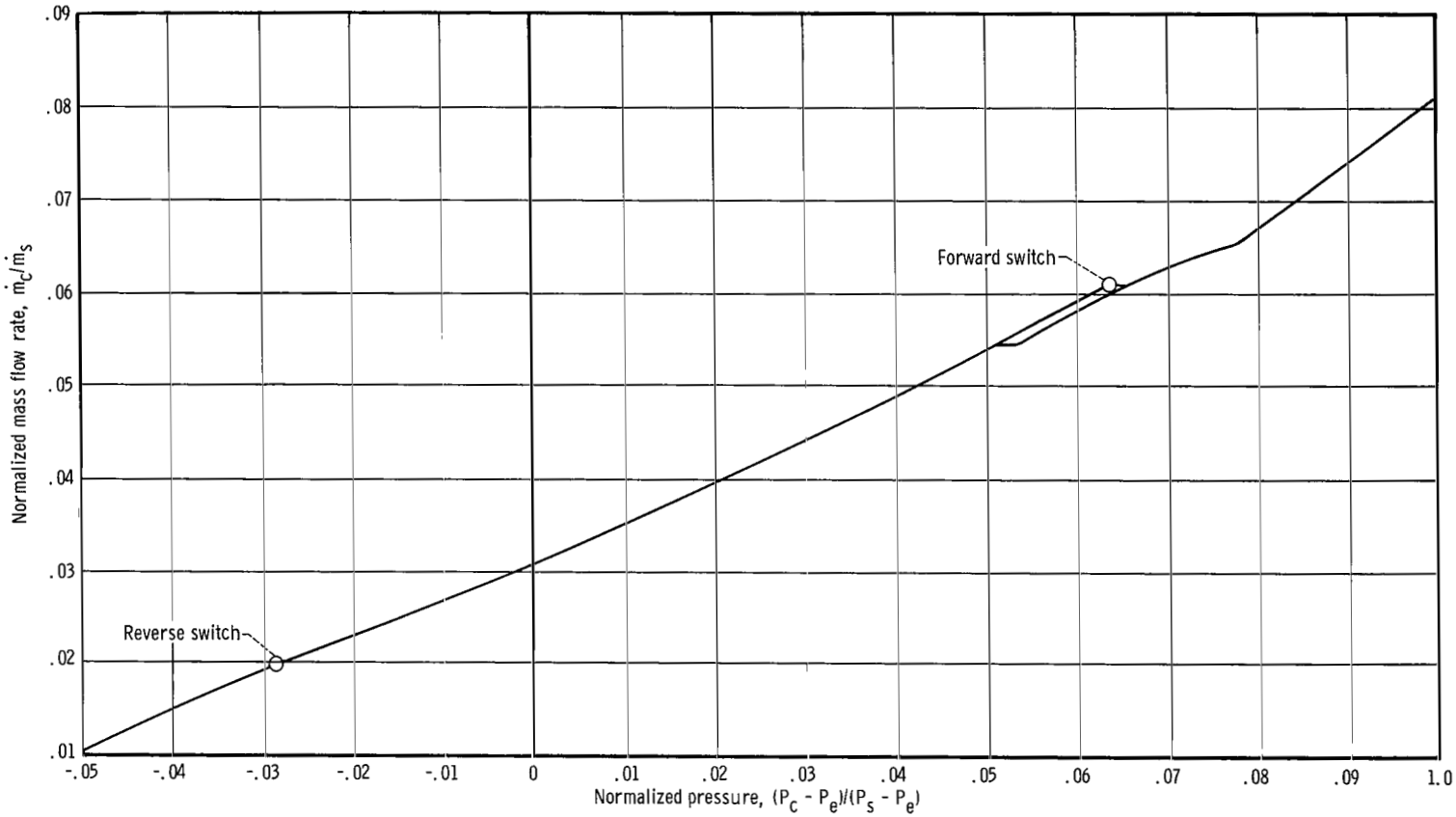

Figure 11. - Control-port pressure-flow characteristics of Lewis SB-1 fluid jet amplifier.

To be noted are the short bellows charging time constant of 0.008 second and the rather large internal volume which the amplifier must drive. Figure 10 shows oscilloscope traces of the bellows pressure as a function of time. As can be seen, the experimental time constant is close to the theoretical, thus indicating validity of the procedures used to predict the bellows charging times and, hence, the required amplifier size. Figures 11 and 12 show typical pressure-flow characteristics of the amplifier control ports and receivers.

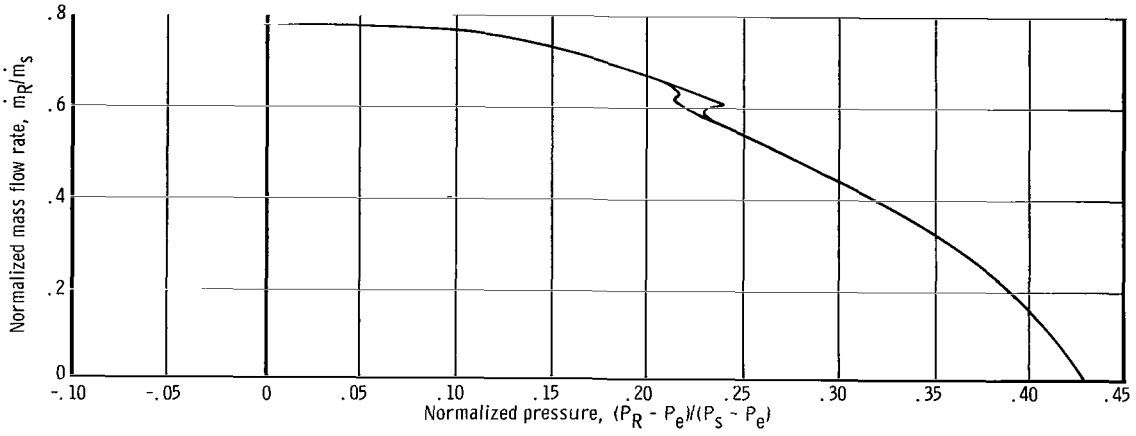

Figure 12. - Receiver pressure-flow characteristics of Lewis SB-1 fluid jet amplifier.

BREADBOARD ACTUATOR SYSTEM

To establish the practicality of the previously discussed circuits, the bellows drive circuitry was implemented, in breadboard form, and connected to the stepping motor to form a complete breadboard actuator system. The resultant system is shown in figure 13, and its design performance specifications are listed in table II.

Breadboard Bellows Drive Circuitry

Except for the power amplifiers, the breadboard implementation of the bellows drive circuitry used standard, commercially available fluid jet amplifiers. The commercial fluid jet amplifiers were made of photoetched ceramic and had barbed hose fittings for input-output connections. All OR units (including those acting as passive

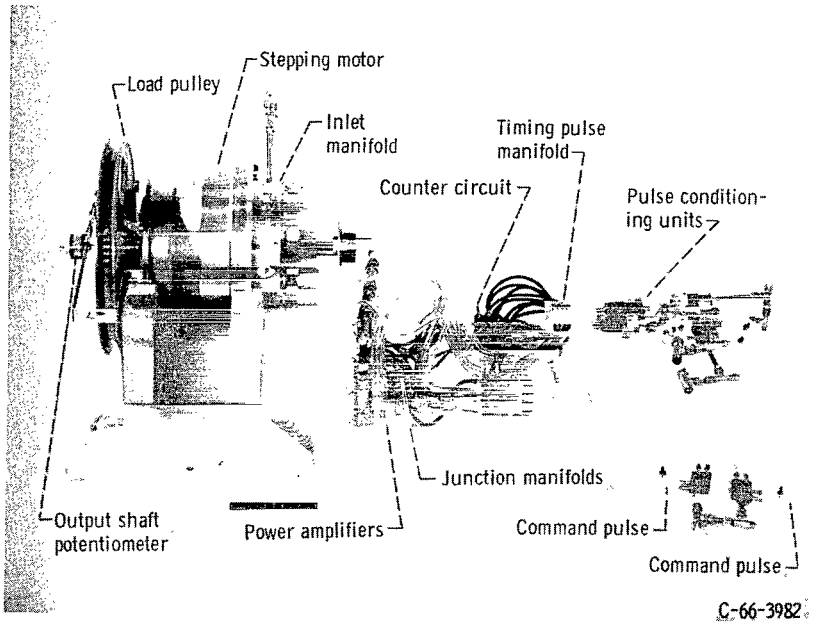

Figure 13. - Breadboard actuator system.

TABLE II. - DESIGN PERFORMANCE SPECIFICATIONS FOR BREADBOARD ACTUATOR SYSTEM

Working fluid	Air
Ambient temperature, ^{o}R (^{o}K)	530 (295)
Supply pressures, psia (N/cm^2)	
Power valves	59.5 (41.1)
Counter circuit	26.7 (18.4)
Pulse conditioning unit	
Amplifier 3	17.7 (12.2)
Amplifiers 1, 2, and 4	20.7 (14.4)
Exhaust pressure (all components), psia (N/cm^2)	14.7 (10.2)
Maximum output torque, in.-lb force (cm-N)	103 (1165)
Load inertia, lb mass-$in.^2$ ($kg-cm^2$)	28 (82.5)
Maximum stepping rate, steps/sec	160
Peak-to-peak (2^{o}) amplitude response, cps	7
Bellows internal volume, $in.^3$ (cm^3)	0.237 (3.89)
Bellows stroke, in. (cm)	0 070 (0.178)
Bellows charging time constant, sec	0.008
Bellows actuating pressure, psid (N/cm^2 differential)	20.5 (14.1)
Total manifolding volume per bellows (calculated), ($in.^3$, cm^3)	0.339 (5.56)
Step size, deg	0.25

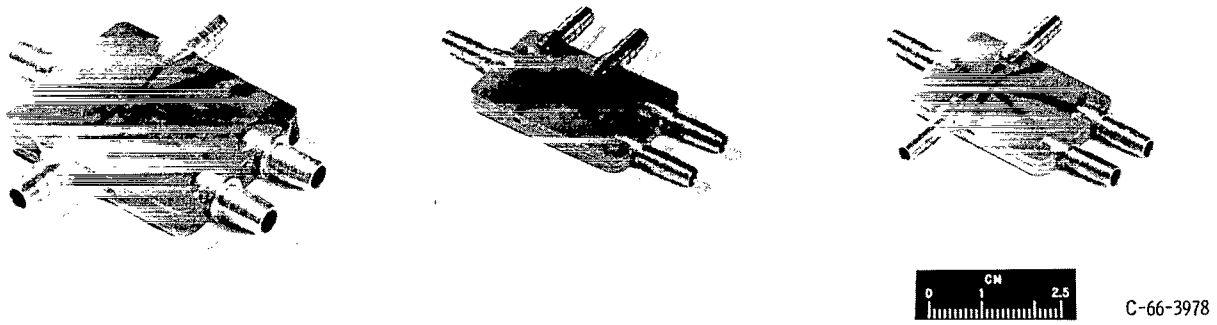

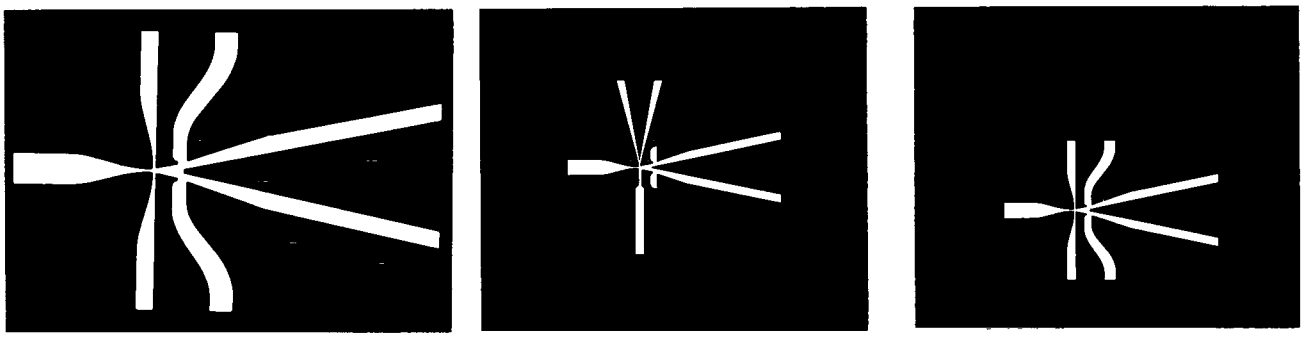

(a) Bistable amplifier; power nozzle, 0.020 by 0.080 inch (0.0508 by 0.204 cm).

(b) OR-NOR unit; power nozzle, 0.010 by 0.040 inch (0.0254 by 0.102 cm).

(c) Small bistable amplifier; power nozzle, 0.010 by 0.040 inch (0.0254 by 0.102 cm).

Figure 14. - Fluid jet amplifiers used in breadboard actuator system and silhouettes.

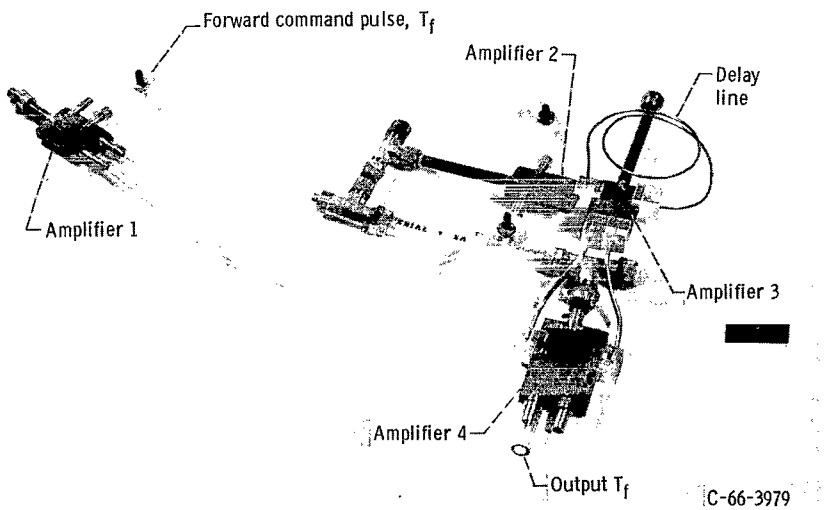

Figure 15. - Pulse conditioning unit.

AND units) were of the asymmetrical wall-attachment type and had a 0.010- by 0.040-inch power nozzle. The central bistable amplifiers (I, II, III, and IV) of the counter and the bistable amplifiers (2, 3, and 4) of the pulse conditioning unit were symmetrical wall-attachment units. The central bistable units and amplifier 4 of the pulse conditioning unit had a 0.020- by 0.080-inch (0.0508- by 0.203-cm) power nozzle. All other amplifiers had a 0.010- by 0.040-inch (0.0254- by 0.101-cm) power nozzle. Figure 14 shows the units as delivered and the manufacturer's silhouettes for the elements.

Figure 15 shows the pulse conditioning unit. Design of the input orifice and delay line of the pulse width fixation portion is somewhat involved and is discussed in detail in appendix C.

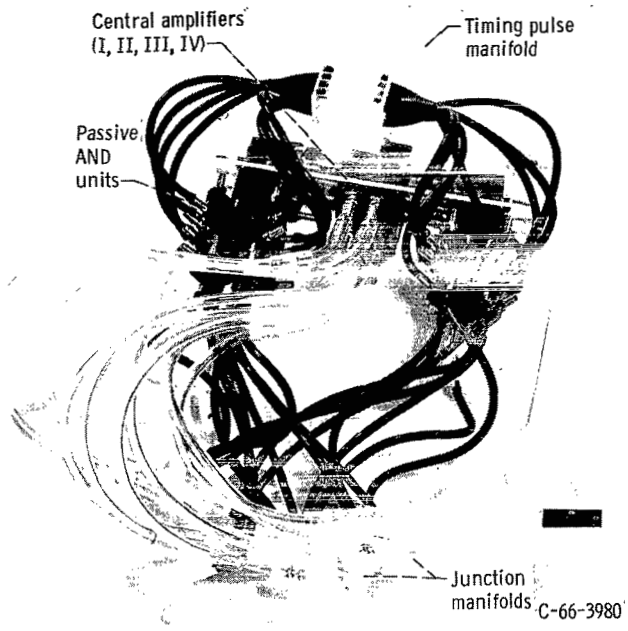

Figure 16. - Breadboard counter circuit.

The counter circuit is shown in figure 16. Each central bistable unit (I, II, III, and IV) with its associated OR units forms a single layer of seven elements. Four such layers are stacked on top of each other to form the complete counter circuit. A manifold is used to distribute the timing pulses, T_f and T_b, as received from the outputs of the pulse generator. The output of the central bistable amplifiers is fed to junction manifolds which are located on and pressurize the control ports of the power amplifiers. From the control ports of the power amplifiers, the output signals from amplifiers I, II, III, and IV are fed back to the supply nozzles of the various passive AND units in the counter circuit proper.

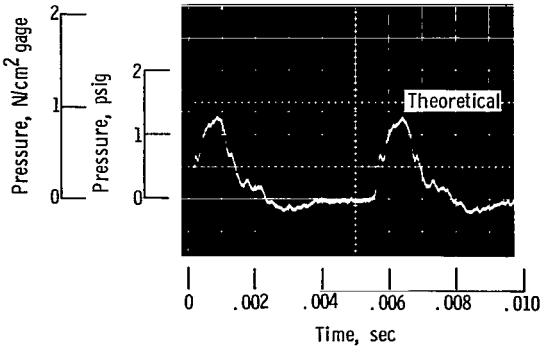

Figure 17. - Timing pulse delivered to control port of passive AND unit. Supply pressure to pulse conditioning unit, 6.0 psig (4.14 N/cm^2 gage).

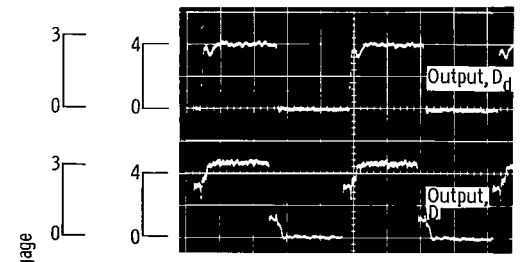

(a) Circuit pressure, 12.0 psig (8.3 N/cm^2 gage).

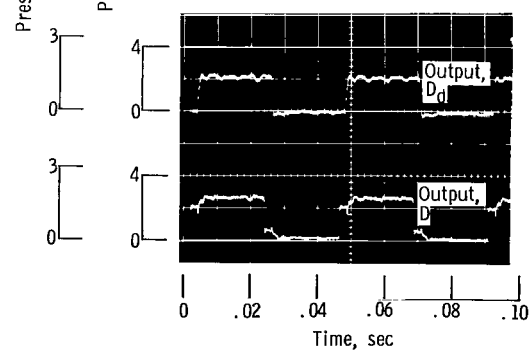

(b) Circuit pressure, 6.0 psig (4.15 N/cm^2 gage).

Figure 18. - Counter outputs D and D_d.

Of interest is an interconnection technique used to reduce signal attenuation to the transmission lines of the counter circuit. If a driving source characteristic typical of most fluid jet amplifiers is used, it is often possible to find an oversized transmission line in which the pulse reflected by the load is completely cancelled by the driving source impedance. By this method, it is possible to deliver a pulse of proper waveform to the load with an oversized line and thus incur much lower frictional losses than if an acoustically matched line were used. This technique, which might be termed "single reflection termination," is described in appendix B and was used to size both the lines used to distribute the timing pulse and those used to carry the counter outputs to the power nozzles of the passive AND units. Figures 17 and 18 show oscilloscope traces of the timing pulse and the carry signal D, respectively. The height and width of the timing pulse are close to the theoretical values. The small steps before and after the pulse result from the pressure transducer being mounted about 1 inch (2.54 cm) away from the interaction region of the AND unit. The delayed carry signal $D_{delayed}$, has sharp rise and decay times and is also of proper height and width. To be noted is the presence of the reflected wave in the source (output D). A detailed analysis of these waves is given in appendix B.

Experimental Performance of Breadboard Actuator System

A series of performance tests was conducted on the complete breadboard actuation system to determine the ability of the bellows drive circuitry to drive the stepping motor. As shown in figure 19, the output shaft could be stepped in either direction at 173 steps per second. Rather small, periodic waviness occurred on the otherwise smooth output trace. To investigate the source of waviness, the actuator was stepped at slower speeds and photographs were made of oscilloscope traces of the shaft position. As shown in figure 20, the step sizes are nonuniform. Once every eight steps, a large step of approximately 0.4° occurs. As the stepping rate is increased, the smaller steps smooth out, but the large step remains. The actuator was disassembled and inspected for obvious flaws, such as dirt between the gear teeth or damaged bellows, which might cause such a change in step size. None were found, and the cause of the uneven steps remains unexplained.

Analogous to the frequency response test performed on proportional actuators, the stepping motor can be commanded to cyclicly reverse direction after a fixed number of steps. As shown in figure 21, the inertially loaded actuator system can be cyclicly stepped eight steps (2°) in each direction without missing, at a stepping rate of 115 steps per second. This performance is roughly comparable to a bandwidth of 7.2 cps at $\pm 1^{\circ}$ amplitude for a conventional piston actuator.

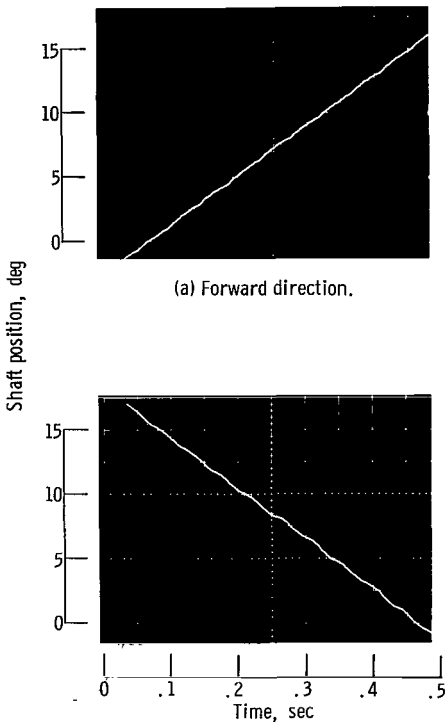

(a) Forward direction.

(b) Backward direction.

Figure 19. - Output shaft position as function of time at 173 steps per second.

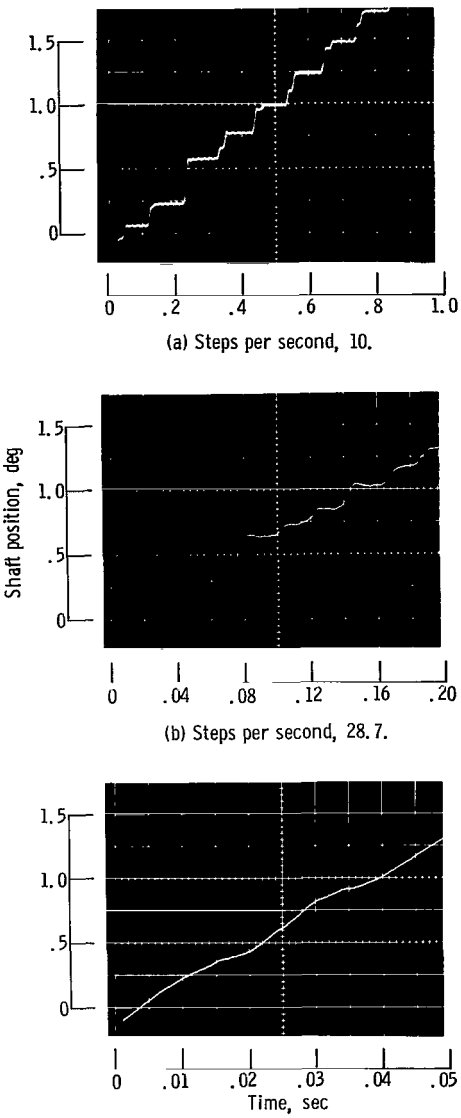

(a) Steps per second, 10.

(b) Steps per second, 28.7.

(c) Steps per second, 115.

Figure 20. - Output shaft position as function of time. Steady stepping rate.

Maximum output torque was measured by increasing the load torque on the actuator output shaft while the actuator was being stepped until the driving gear would disengage. The results shown in figure 22, indicate a maximum static output torque of 70 inch-pounds force (789 cm-N) and a maximum slewing rate of approximately 37^{o} per second. The reduction in output torque from the design value of 103 inch-pounds force (1165 cm-N) can be attributed to (1) the inherent stiffness of the bellows and driving gear gimbal flexures and (2) the fact that the differential output pressures of the power amplifiers

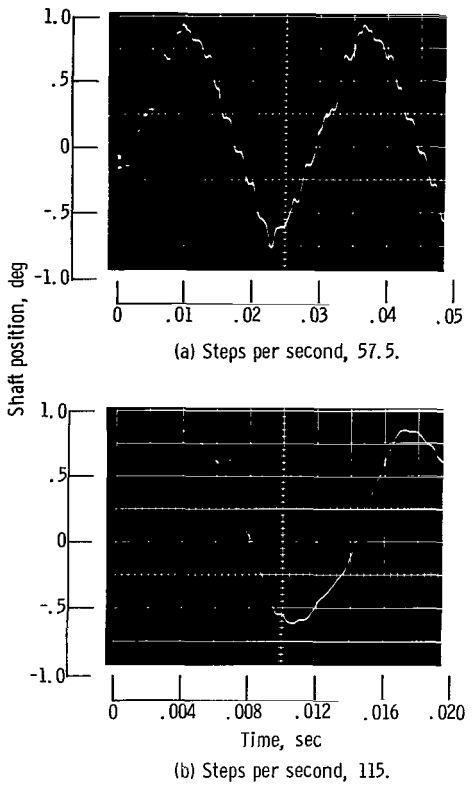

Figure 21. - Small amplitude response of breadboard actuator system. Eight steps each direction.

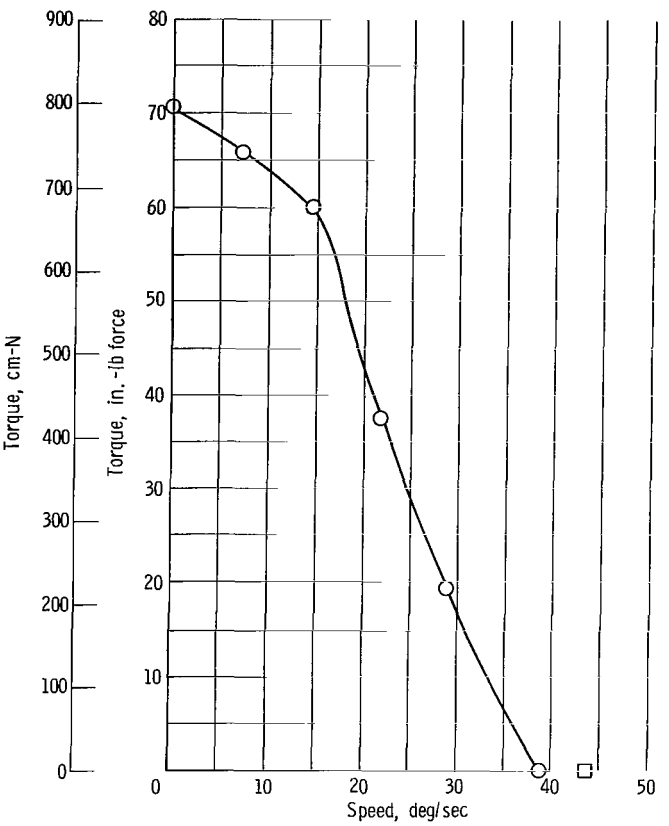

Figure 22. - Output torque as function of speed of breadboard actuator system.

were somewhat lower than the 20.5 psi (14.1 N/cm^2) design value. A differential bellows pressure of 4 psi (2.76 N/cm^2) was required to force the nutating gear into contact with the output gear. Subtracting this pressure from the 18 psi (12.4 N/cm^2) differential pressure experimentally delivered by the drive circuitry power amplifiers and then dividing by the 20.5 design value output pressure for the breadboard circuit (table II) yields the following predicted reduction in output torque:

$$\eta = \frac{18.0 - 4.0}{20.5} = 0.683$$

This reduction indicates an experimental output torque of 0.683 times 103 or 70.3 inch-pounds force (800 cm-N), which is approximately that observed. Since the stepping motor is designed for a bellows differential operating pressure of 70 psi (48.3 N/cm^2), the torque efficiency can be increased by raising the bellows actuating pressures to this value. This increase may be accomplished by increasing both the supply and exhaust pressures of the bellows drive circuitry. A prototype bellows drive circuit operating at NERVA supply and exhaust pressures of 200 psia and 50 psia (138 and 33.5 N/cm^2 abs), respectively, would deliver a differential output pressure of approximately 61.3 psi

(42.5 N/cm^2) to the bellows. The output torque, under such conditions, would probably rise to 82 percent of its design value.

The reduction in maximum, unloaded slewing velocity observed in the torque-speed tests has not been explained but probably results from interactions between the actuator and the large load pulley used for applying torques. When the rated load inertia of 28 pounds mass-inch squared (82.5 (kg)(cm^2)) was replaced on the actuator output shaft, the actuator could again be operated in both directions at 43.3° per second or 173 steps per second (shown by the solid symbol in fig. 22).

COMPARISON OF BREADBOARD NUTATOR ACTUATOR SYSTEM WITH CONVENTIONAL PISTON ACTUATOR

Although the nutator actuator system has a unique set of characteristics which make it inherently well adapted to some applications and less well adapted to others, it is instructive to compare it with the more conventional piston actuator. The piston actuator is considered to be frictionless, driven by a flapper valve, and to have a theoretical performance at least equal to that of the ideal performance of the breadboard actuator system (table II). The flows required by the actuator systems, their maximum output torques, and their maximum slewing velocities are used as the criteria of comparison. Two cases are considered for the stepping-motor system: the first is with a power amplifier load volume equal to that calculated for the breadboard actuator system (0.576 in.^{3}; 9.4 cm^3), the other is with a power amplifier load volume equal to the bellows load volume of 0.237 cubic inch (3.88 cm^3) plus the internal volume of a channel 1/16 inch square by 7.5 inches long (0.159 by 19.1 cm). The latter volume is considered to be the minimum practical manifolding volume that could be obtained in a prototype actuator system. The flow required by the prototype actuator system was determined by first computing the flow required by the power valves and then scaling the rest of the logic-circuitry flow in proportion to the power-valve flow.

The results of comparing the two systems are as follows:

Design performance specifications:

Working fluid	Air at 530° R (294° K)
Supply pressure, psia (N/cm^2)	59.7 (41.2)
Exhaust pressure, psia (N/cm^2)	14.7 (10.3)
Maximum output torque, in.-lb force (cm-N)	103 (1165)
Resolution, deg	±0.25
Maximum slewing rate, deg/sec	40
Load inertia, lb mass-in.^{2} (kg-cm^2)	28.0 (82.5)
Frequency response, 2° peak-to-peak amplitude, cps	Flat to 7

Actual stepping-motor system performance:

Maximum output torque, in.-lb force (cm-N)	70 (789)
Resolution, deg	±0.25
Maximum slewing rate, deg/sec	43.3
Frequency response, 2° peak-to-peak amplitude, cps	7.2

Hypothetical piston actuator performance:

Maximum output torque, in.-lb force (cm-N)	103 (1165)
Maximum slewing rate, deg/sec	99.5
Frequency response, 2° peak-to-peak amplitude, cps	7

Total system flow consumption:

Hypothetical piston actuator	
lb mass/sec (kg/sec)	0.00071 (0.000321)
standard ft^3/min (standard m^3/min	0.945 (0.0268)
Breadboard stepping-motor system (Load volume per bellows, 0.576 in.^{3} or 9.4 cm^3)	
lb mass/sec (kg/sec)	0.0211 (0.00955)
standard ft^3/min (standard m^3/min)	16.9 (0.479)
Prototype stepping-motor system (Load volume per bellows, 0.266 in.^{3} or 4.36 cm^3)	
lb mass/sec (kg/sec)	0.01035 (0.00469)
standard ft^3/sec (standard m^3/sec)	8.3 (0.235)

As can be seen, the primary disadvantages of the stepping-motor system are flow consumption and maximum slewing speed. The breadboard system consumes 29.7 times as much flow as an equivalent piston actuator, while the prototype system consumes 14.6 times as much. It is possible to further reduce flows required by the prototype system (1) if higher-pressure recovery power valves are used, thus permitting smaller bellows, (2) if the bellows stiffness is reduced, thus permitting the same output torques for a lower power-valve supply pressure, (3) if a larger bellows charging time constant can be allowed, thus permitting smaller power amplifiers, and (4) if either the bellows volume or line manifolding volume is reduced. The last approach could yield large

decreases in power amplifier flow consumption, since the bellows charging flows outweigh displacement flows by a factor of 8.2. Reduction of the bellows volume, however, will probably be a difficult task since approximately half of their internal volume already is eliminated by an insert.

CONCLUSIONS

From an investigation of a breadboard flueric-controlled pneumatic stepping-motor system, the following conclusions were drawn:

1. The fluid jet amplifier bellows drive circuitry is sufficiently fast that bellows charging time is the primary limitation to the maximum stepping-motor-system speed. Although it has not been tested at higher rates, we believe that the current bellows drive circuitry can operate satisfactorily at well above 173 steps per second.

2. The improved bellows drive circuitry and the stepping motor constitute a reliable, open-loop stepping actuator system with inherently high output stiffness, reasonable slewing speeds, and small step size. Further improvements in both the actuator and the power valves of the bellows drive circuitry should increase system performance beyond that reported herein.

3. The stepping-motor-system flow consumption will be much higher than that of an equivalent flapper-valve-driven piston actuator designed to do the same job. However, for many aerospace applications, this disadvantage in flow consumption may not be large in comparison to the advantages in simplicity, apparent reliability, and high output stiffness that are offered by the pneumatic stepping motor in combination with a flueric digital drive system.

Lewis Research Center,
National Aeronautics and Space Administration,
Cleveland, Ohio, October 6, 1967,
122-29-03-09-22.

APPENDIX A

SYMBOLS

A	line area
A*	equivalent choked nozzle area
A, B, C, D	output of counter
C_1, C_2	amplifier control ports
c	speed of sound, in./sec; cm/sec
D	line diameter, in.; cm
D_n	width of power nozzle exit, in.; cm
g_o	acceleration of gravity, (lb mass)(in.)/(lb force)(sec^2); (kg)(cm)/(N)(sec^2)
k	ratio of specific heats
ℓ	length of line, in.; cm
$\dot{m}$	mass flow rate, lb mass/sec; kg/sec
m_n	2n + 1, eq. (E19)
n	dummy index
P	pressure, lb force/$in.^2$; N/cm^2
R	Reset
R_1, R_2	amplifier receivers
$\mathcal{R}$	line resistance per unit length, (lb force)(sec)/(lb mass)($in.^3$); (N)(sec)/(kg)(cm^3)
$\mathcal{R}_{tot}$	total line resistance, (lb force)(sec)/(lb mass)($in.^2$); (N)(sec)/(kg)(cm^2)
r	reflection coefficient
S	Set
s	Laplacian operator, sec^{-1}; supply
T	timing pulse; torque, in.-lb force; cm-N
t	time, sec
V	vent
x	distance down line, in.; cm

$y(s)$	line shunt admittance per unit length, (lb mass)(in.)/(lb force)(sec); (kg)(cm)/(N)(sec)
Z	impedance, (lb force)(sec)/(lb mass)(in.^{2}); (N)(sec)/(kg)(cm^2)
$Z(s)$	line series inertness per unit length, (lb force)(sec)/(lb mass)(in.^{3})
$Z_c(s)$	total line surge impedance, (lb force)(sec)/(lb mass)(in.^{2}); (N)(sec)/(kg)(cm^2)
Z_{co}	line surge impedance in absence of friction, (lb force)(sec)/(lb mass)(in.^{2}); (N)(sec)/(kg)(cm^2)
α	attenuation term in transmission-line equations
η	torque efficiency
$\Gamma(s)$	propagation operator
μ	viscosity, (lb force)(sec)/(in.^{2}); (N)(sec)/(cm^2)
ρ	density, lb mass/in.^{3}; kg/cm^3
τ	time delay, sec
I, II, III, IV	central bistable amplifiers
Subscripts:	
A, B, C, D	Boolean variables
a	start of line
b	backward, end of line
1, 2, 3	amplifiers in counter circuit (identified in app. B)
c	control, characteristic value
d	delayed
e	exhaust
f	forward
j	jet
l	line
o	reference conditions
q	quiet
R	receiver
R_1, R_2	amplifier receivers

s supply

sw switching

t transmission line

x conditions before wave in line

y conditions after wave in line

Superscripts:

(-) logical complement of quantity

(') dimensionless impedance or resistance, compressible flow in amplifier

('') dimensionless impedance or resistance incompressible flow in amplifier

APPENDIX B

SIMPLIFIED INTERCONNECTION TECHNIQUES FOR DIGITAL FLUID JET AMPLIFIERS

This discussion of some simplified techniques for interconnection of digital fluid jet amplifiers is included as an aid for understanding both appendix C and the pulse reflection technique used to minimize steady-state viscous flow losses in a transmission line.

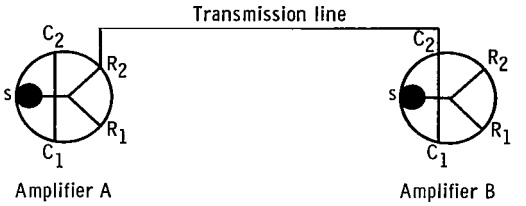

Figure 23. - Typical interconnection of two bistable fluid jet amplifiers.

The interconnection problem is illustrated schematically in figure 23. The output of a bistable fluid jet amplifier is connected to a transmission line which, in turn, feeds the control port of a second bistable amplifier. Amplifier A initially has its output directed through its receiver R_1, while amplifier B has its output directed to its receiver R_2. If amplifier A is switched to its receiver R_2, a pressure pulse will be sent down the line. If the control-port impedance of amplifier B does not completely absorb this pulse, reflected waves will be sent up and down the line. A change in the control-port impedance of amplifier B during this process, as a result of switching, will further complicate the situation.

A rigorous analysis of the transmission line, by itself, is involved and, when coupled with the nonlinear input-output characteristics and dynamics of the fluid jet amplifiers, this task becomes formidable. Fortunately, however, the flueric transmission lines used in many practical engineering situations are sufficiently short that friction and pulse dispersion may be either neglected or considered to be small. Also, for well-designed fluid jet amplifiers, the switching dynamics of the amplifier are fast in comparison to the transit times of the pulses sent down the lines. This fast switching permits the amplifiers to be regarded as two state, nonlinear sources and loads.

With the foregoing assumptions of low line friction and fast amplifier switching, the analysis of digital fluid jet amplifier interconnection may be considerably simplified. In the case of zero line friction or pulse dispersion, the transmission line may be modelled as a pure, bilateral delay unit with equal input and output characteristic impedances of magnitude:

$$Z_{co} = \left(\frac{\rho_y}{\rho_x}\right)\left(\frac{C}{A_l g_o}\right) = \frac{\Delta P}{\dot{m}} \tag{B1}$$

where ρ_y/ρ_x is the ratio of the fluid densities after and before the wave sent down the tube, respectively. Since the input-output pressure-flow characteristics of fluid jet amplifiers are often plotted in normalized form, it is convenient to normalize equation (B1) with respect to the power nozzle pressures and flows of the fluid jet amplifier driving it. Equation (B1) may be rewritten as follows:

$$Z'_{co} = \left(\frac{P - P_e}{P_s - P_e}\right)\left(\frac{1}{\frac{\dot{m}}{\dot{m}_s}}\right) = \frac{k\left(\frac{\rho_y}{\rho_x}\right)\sqrt{\left[\left(\frac{2}{k+1}\right)^{(k+1)/(k-1)}\right]}}{\frac{A_l}{A_j}\left(1 - \frac{P_e}{P_s}\right)\frac{A_j}{A^*}} \tag{B2a}$$

For air,

$$Z'_{co} = \frac{0.813\left(\frac{\rho_y}{\rho_x}\right)}{\left(\frac{A_l}{A_j}\right)\left(1 - \frac{P_e}{P_s}\right)\left(\frac{A_j}{A^*}\right)} \tag{B2b}$$

For approximately incompressible power nozzle flow (<3.0 psig (2.07 N/cm^2 gage) supply for atmospheric exhaust), equation (B2a) reduces to

$$Z''_{co} = \left(\frac{P - P_e}{P_s - P_e}\right)\left(\frac{1}{\frac{\dot{m}}{\dot{m}_s}}\right) = \left(\frac{2kP_s}{P_s - P_e}\right)^{1/2}\left(\frac{\frac{\rho_y}{\rho_x}}{\frac{A_l}{A_j}}\right) \tag{B3}$$

A first approximation to the time history of the waves and pressures in the transmission line of figure 23 can now be obtained. The pressure flow characteristics of the driving-amplifier output and the driven-amplifier input (control port) are plotted on the same graph, as shown in figure 24. Intersection 1 denotes the steady-state conditions before amplifier A is switched into the line and intersection N denotes steady-state

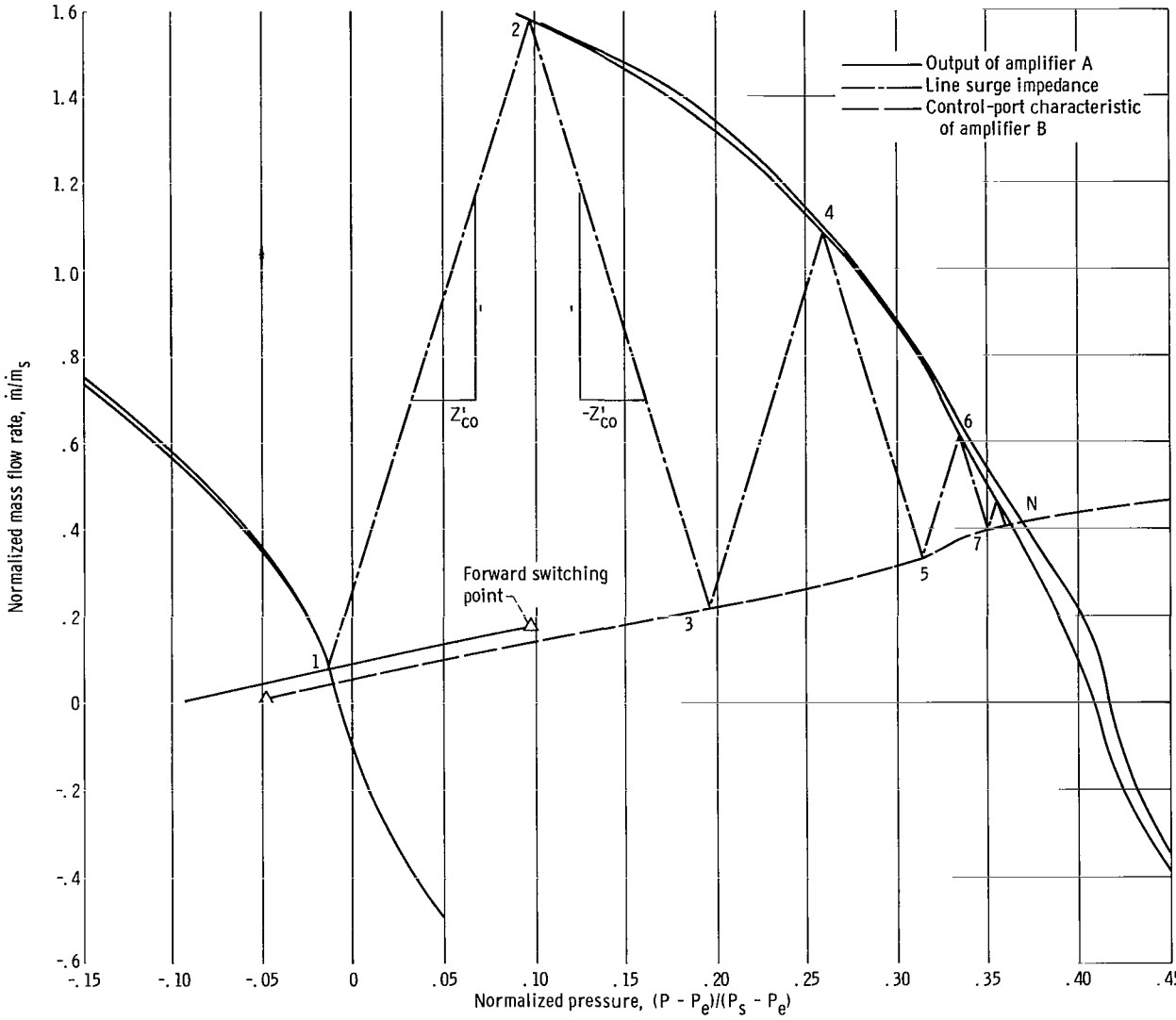

Figure 24. - Load-line solution to transmission-line pressures.

conditions after all transients have died out. The surge impedance of the line has no effect on the location of these two steady-state operating points.

Between these two steady-state conditions, however, the transmission-line dynmics come into play. During the transient in which amplifier A is switched into the line, the frictionless line initially appears as a resistive impedance Z'_{co} which is slightly nonlinear as a result of the ρ_y/ρ_x term in equations (B1) to (B3). For most practical engineering cases, this nonlinearity is small and will be neglected. Thus, as shown in figure 24, a pulse of pressure and flow indicated by intersection 2 is sent down the line. At the end of the line, the pressure pulse meets the terminating load impedance. If the pressure and flow carried by the initial pulse are not compatible with the pressure-flow

characteristics of the terminating impedance, a readjustment of flow conditions at the end of the line must occur. To the load, the line behaves as a source with impedance $-Z'_{co}$ (since positive flow is now defined as being out of the line) which has initial pressures and flows specified by intersection 2 of figure 24. Thus, the pressure at the end of the line will increase and flow will decrease until they reach a value compatible with the pressure-flow characteristics of the load (intersection 3, fig. 24). These new flow conditions, however, differ from the pulse initially sent down the line. Thus, a pressure pulse is sent up the line to the receiver of the driving amplifier A. Again, the new conditions represented by intersection 3 are not acceptable to the receiver of amplifier A and another readjustment takes place, at intersection 4. Reflections continue to occur until the final steady state is reached.

If a transmission line is used which intersects the receiver output characteristics at the same points as do the load characteristics (dashed line, impedance Z'_1, fig. 25), no

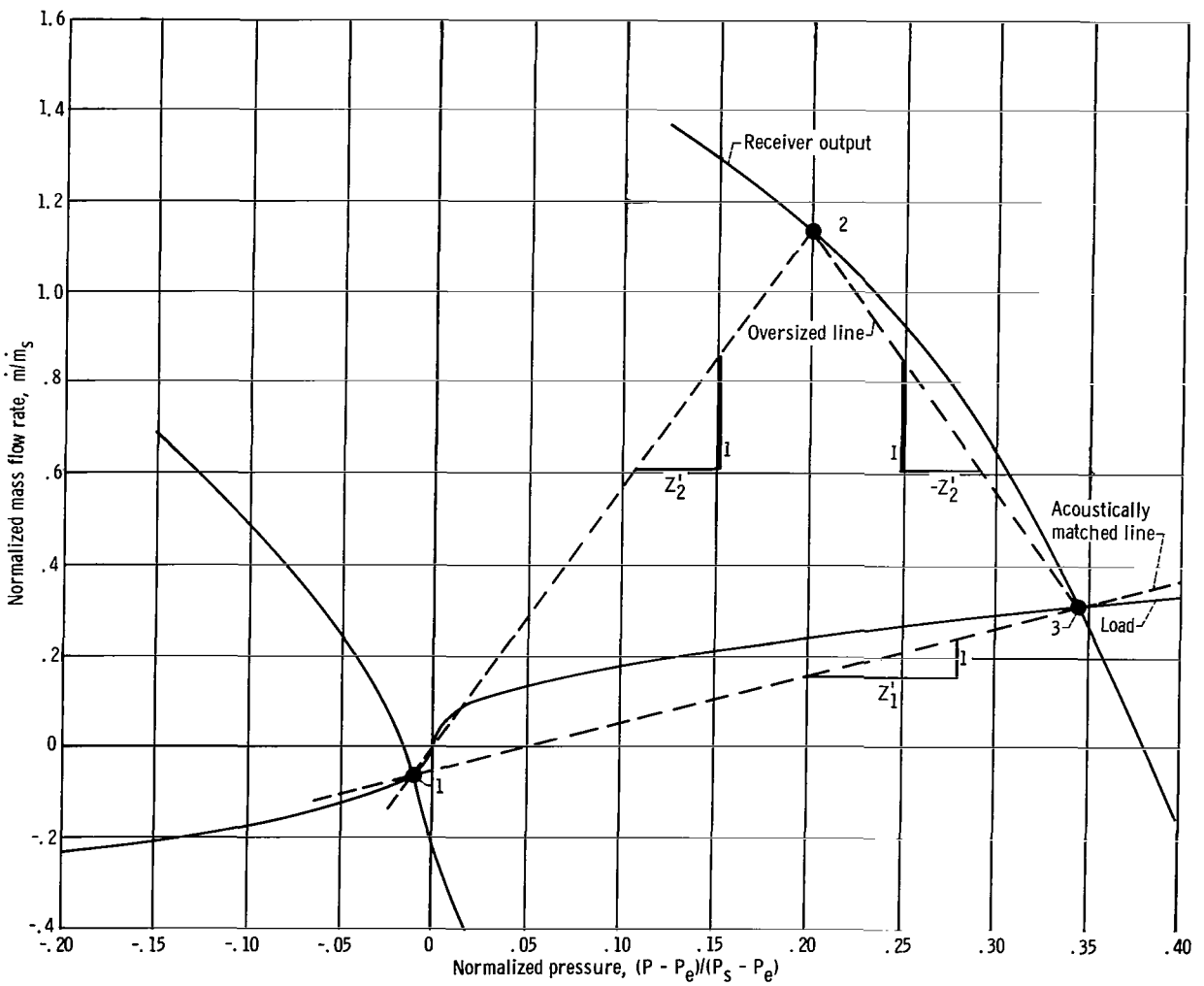

Figure 25. - Single-reflection line termination technique.

reflected pulse will be necessary to readjust flow conditions at the end of the line. Steady-state conditions will exist after passage of the initial switching pulse. A second case can be considered in which the transmission line is oversized (impedance Z'_2, fig. 25) but intersects the receiver output characteristics at a point (intersection 2, fig. 25) such that the reflected pulse readjusts flow conditions in the line to the final, steady-state value (intersection 3, fig. 25). In the absence of wave-form distortion due to the effects of friction, the pulse delivered to the load will be indistinguishable from that delivered by an acoustically matched line since, to the load, the reflected wave is not a separate pulse. This technique enables properly shaped pulses to be delivered to loads by oversized transmission lines. The oversized lines, because of their larger internal diameter, will have much lower frictional losses and pulse dispersion than lines acoustically matched to load impedances.

The presence of friction in the line, even in small amounts, complicates the situation. Steady-state viscous flow losses may be approximated by the equation for Hagen-Poiseuille flow in a pipe:

$$P_a - P_b \simeq \frac{128\,\dot{m}\mu l}{\rho_l \pi D^4} \tag{B4}$$

which, when normalized to the power nozzle pressures and flows of the driving amplifier is expressed as

$$R' = \left(\frac{\Delta P}{P_s - P_e}\right)\left(\frac{1}{\frac{\dot{m}}{\dot{m}_s}}\right) = Z'_{co}\left(\frac{8\pi\mu c_o l}{kP_e A_l}\right) \tag{B5}$$

or, for approximately incompressible power nozzle flow as

$$R'' = \left(\frac{\Delta P}{P_s - P_e}\right)\left(\frac{1}{\frac{\dot{m}}{\dot{m}_s}}\right) = Z''_{co}\left(\frac{8\pi\mu c_o l}{kP_e A_l}\right) \tag{B6}$$

Although equations (B4), (B5), and (B6) predict steady-state losses, they do not accurately account for the effects of friction when the pulse is travelling in the line. A simplified analysis of these effects is given in appendix D for the case of an acoustically terminated line of low internal friction (10 percent of its surge impedance). The results indicate that if a step change in pressure is applied to one end of the line, attenuation of

the pulse at the time it reaches the other end of the line will be half the final, steady-state value. After a period of time equal to two transit times of the line has elapsed, the losses will have risen to their final steady-state value. If these results can be generalized to the nonacoustically terminated line, then, for the following cases, it would appear possible to treat the effects of friction approximately by constructing an equivalent source.

(1) If the pulse duration is short in comparison to one line transit time, the equivalent source would be equal to the actual driving source with one-half the steady-state losses subtracted.

(2) If the pulse duration was equal to or greater than two line transit times, the equivalent source would be the driving source minus the steady-state frictional losses. In both cases, the transmission line would be treated as if it were frictionless and the source - transmission line - load interactions would be analyzed in the same manner as was done in figure 3.

The analysis in appendix D is based on electrical transmission-line theory and only approximates conditions in a pneumatic transmission line. The results, therefore, are not highly accurate and the analysis should only be used to indicate whether or not a transmission line has acceptable or unacceptable losses. For many engineering applications, however, such information is sufficient. The corrections used to reduce losses usually reduce them by factors of two or more. In comparison with the error that might occur in the predicted losses, the corrective changes are large.

The technique of subtracting steady-state losses from the driving source and constructing an equivalent source was used to predict the behavior of the timing pulse and the carry signal. As mentioned in the test, eight lines (1/16 in. (0.159 cm) i.d. and 8 in. (20.3 cm) long) were used to carry the timing pulse from amplifier 4 of the pulse conditioning unit to the control ports of the passive AND units. The combined normalized impedance of these lines was

$$Z'_{co} = 0.167$$

and their combined frictional resistance was

$$R' = 0.0169$$

The normalized receiver pressure-flow characteristics of amplifier 4 of the pulse conditioning unit are plotted in figure 26. The dashed lines are the receiver characteristics minus the steady-state frictional pressure drop in the line. On the same plot is shown the combined control-port impedance of the eight passive AND units.

Starting at location 1 in figure 26, the combined timing pulse line impedance is seen

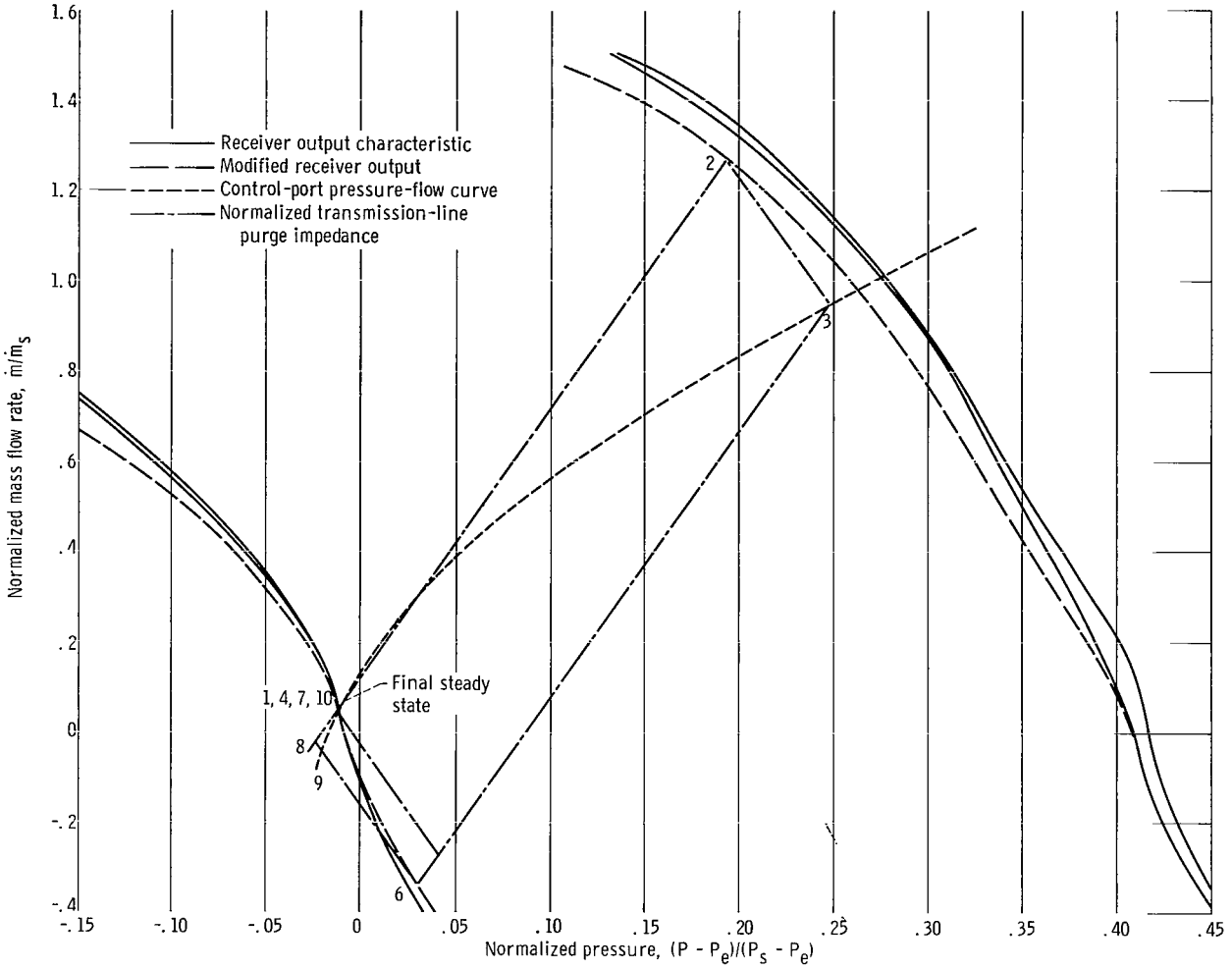

Figure 26. - Trajectory of timing pulse.

to intersect the receiver output characteristics at location 2. Thus, a pressure pulse of approximately 0.19 $(P_s - P_e)$ or 1.14 psi (0.788 N/cm^2) will be sent down the line. At the load, it is reflected as a pressure pulse with a final value of 0.247 $(P_s - P_e)$ or 1.48 psig (1.025 N/cm^2 gage) (location 3).

Determination of the rest of the pressures in the line as a function of time is conviently handled with the aid of the wave diagram shown in figure 27. The diagram is the same as normally used for computations of one-dimensional, unsteady flow (for an example, see Shapiro, ref. 6, vol. II, ch. 23). Position of the wave is plotted as a function of time (vertical axis) and distance along the transmission line (horizontal axis). The different areas in the diagram correspond to conditions in the line at different locations and times. Thus, the initial steady-state conditions in the line are denoted as 1 and occupy the lower right corner of the diagram. As the wave advances down the tube (from left to right in the diagram), conditions change to 2 (the same as intersection 2

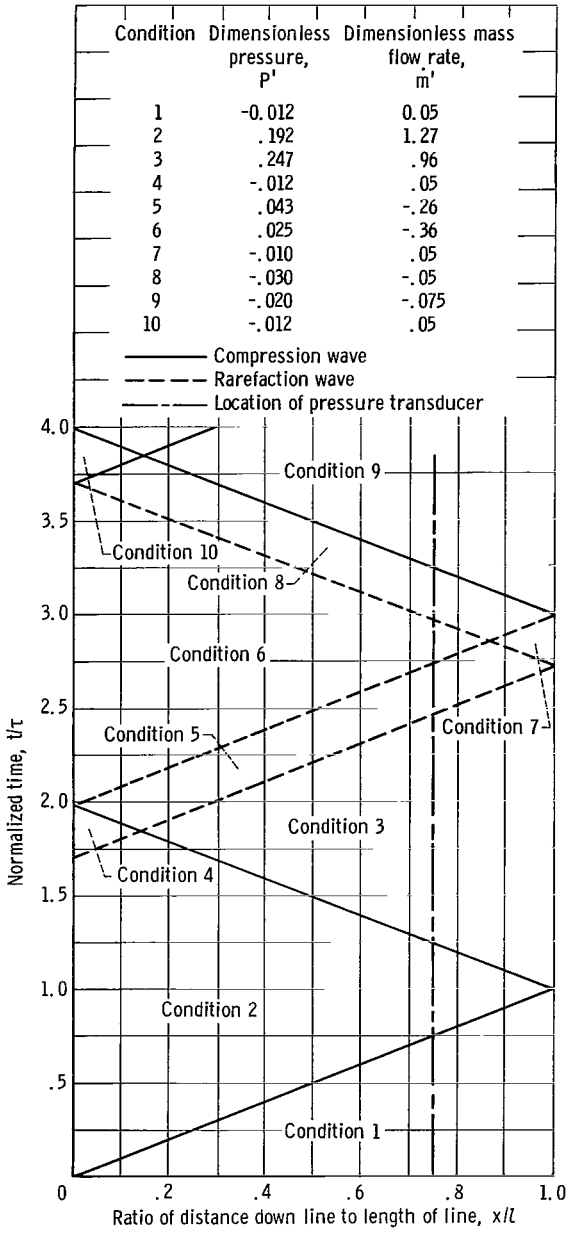

Figure 27. - Wave diagram of timing pulse. Length of line, 8.0 inches (20.3 cm); time delay, 0.588×10^{-3} second.

in fig. 26). Reflection from the right end of the tube (load end) causes a pressure wave to be sent back down the tube with conditions 3 behind it. The output amplifier of the pulse conditioning unit is switched away from the transmission line before the reflected wave has a chance to arrive at its receiver. Thus, the receiver will immediately assume conditions 4 (intersection 4 in fig. 26) since it has no way of knowing that conditions in the line are any different than those specified by intersection 2. Region 5 denotes a condition which is internal to the line and exists only momentarily at the driving amplifier and the control ports of the passive AND units. Condition 5 can be determined analytically by the linearized theory of characteristics (ref. 6) or graphically by use of figure 26. If the theory of characteristics is used, the magnitude of the wave between conditions 2 and 3 is calculated

$$\Delta P' = 0.247 - 0.192 = +0.055$$

$$\Delta \dot{m}' = 0.96 - 1.27 = -0.31$$

and its pressure and flow changes are added to those existing in region 6. Thus, the normalized pressure in region 5 would be

$$P' = -0.012 + 0.055 = 0.043$$

and the normalized flow would be

$$\dot{m}' = 0.05 - 0.31 = -0.26$$

Alternatively, lines of slope Z' and $-Z'_{co}$ may be drawn from intersections 3 and 4, respectively, in figure 27. The intersection of these two lines, intersection 5, represents the same conditions in the line as condition 5 in figure 28. The reason for this can be seen by considering a cut in the transmission line at station x where the waves of intersections 3 and 4 first meet. At the time the waves arrive at this station, the portion of the line to the right of the cut would appear to have the pressures and flows specified by intersection 3 (fig. 26) and an output impedance of Z'_{co}. The portion of the line to the left of the cut would appear to have the pressures and flows of intersection 4 (fig. 26) and an output impedance of $-Z'_{co}$. The pressures and flows that result from the meeting of the two waves must be compatible with these two equivalent sources. Thus, the intersection of the Z'_{co} and $-Z'_{co}$ lines drawn from them represent the only set of conditions mutually acceptable to the two equivalent sources.

Use of figure 26 is most convenient to determine intersections 6 and 7 since the load and source are nonlinear. Conditions 6 at the driving amplifier are specified by an ex-

tension of the line 3-5 to the unswitched receiver characteristics, while conditions 7 at the load are an extension of a line at slope $-Z'_{co}$ from intersection 5 to the control-port pressure-flow curve. The remaining intersections in figures 26 and 27 may be determined in similar manner. The resultant theoretical time histories of the timing pulse at the control port of the AND unit and the pressure transducer used to measure the timing pulse are plotted in figure 28.

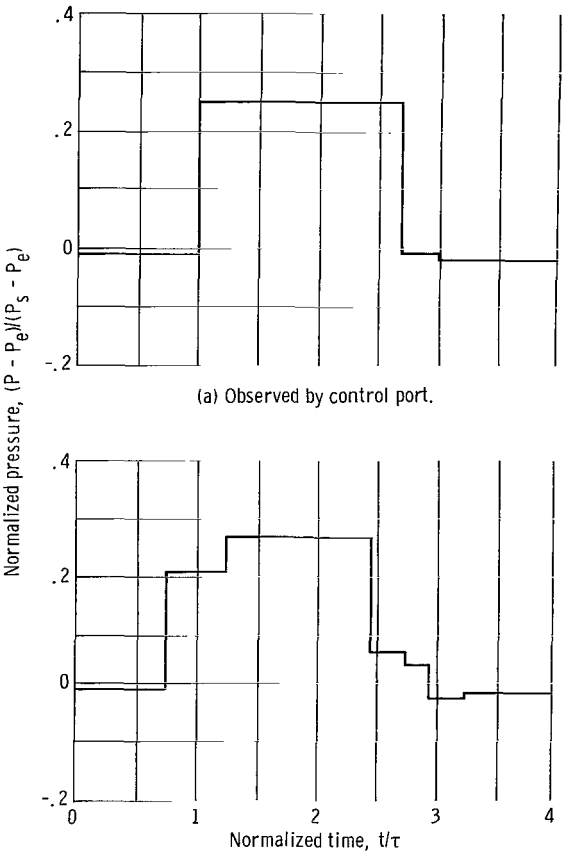

(a) Observed by control port.

(b) Observed by pressure transducer.

Figure 28. - Theoretical timing pulse waveforms.

The experimental timing pulse, shown in figure 17, has a peak amplitude of 1.2 to 1.3 psig (0.829 to 0.896 N/cm^2 gage), a duration of the peak of approximately 0.6 to 0.7 millisecond, and steps at the beginning and end of the pulse of approximately 0.6-psig (0.414-N/cm^2-gage) magnitude. Comparison with the theoretical timing pulse pressure (fig. 28) indicates that the analysis underpredicts steady-state losses and predicts a higher initial wave in the line than was observed. The error in initial wave height suggests that the experimental transmission line had either a larger diameter than assumed or that its walls were highly flexible. A check of the line size indicated that the

actual diameter was close to theoretical. Line elastance was also checked, but contributes only approximately 3.5 percent to the compressibility of the air in the tube. Thus, in this example, the analysis correctly predicted the qualitative shape of the timing pulse waveform and the order of magnitude of the losses, but substantial quantitative errors exist between experiment and theory. However, the predicted pulse attenuation was small enough to be relatively unimportant. If the analysis had predicted a larger pulse attenuation, the lines would have been either shortened or increased in diameter sufficiently to reduce losses to a minimum, thus, again their absolute magnitude would be unimportant.

The carry signal from the central bistable units to the power nozzles of the passive AND units was analyzed in the same manner. The output of each central bistable unit is loaded with one control port of an SB-1 power amplifier and two 1/16-inch- (0.159-cm-) inside diameter rubber lines which feed the power nozzles of two passive AND units. The combined normalized resistance and impedance of the rubber lines are

$$Z'_{co} = 0.469$$

$$R' = 0.0515$$

The control port of the SB-1 amplifier, although located an appreciable distance from the output of the central bistable amplifiers, was considered to be in close contact with them. Thus, the scaled SB-1 control-port characteristics (see appendix E and fig. 11) were subtracted from the outputs of the central bistable units to give an equivalent output (long-dash line, fig. 29). The pressure drops due to line frictional resistance were then subtracted from the new curve to give an equivalent source output (short-dash line, fig. 29) which was used for computation. The first six reflections are shown in the figure.

Figure 29, which shows more than six reflections, does not agree with the waveforms observed on the experimental model (fig. 18, p. 19). The predicted final pressure of 4.0 psig (2.76 N/cm^2 gage) (33 percent of gage supply pressure) is lower than that measured, and the experimental pulse had no observable overshoot. Thus, it would again appear that the line used in the tests had a larger internal diameter than had been assumed in the calculations or that its walls were sufficiently flexible to appreciably decrease its effective acoustical impedance. However, the line used for the carry signals was the same as that used to distribute the timing pulse. Therefore, this suggestion must be regarded as incorrect. In this example, the analysis overpredicted the losses, whereas, in the case of the timing pulse, it underpredicted losses.

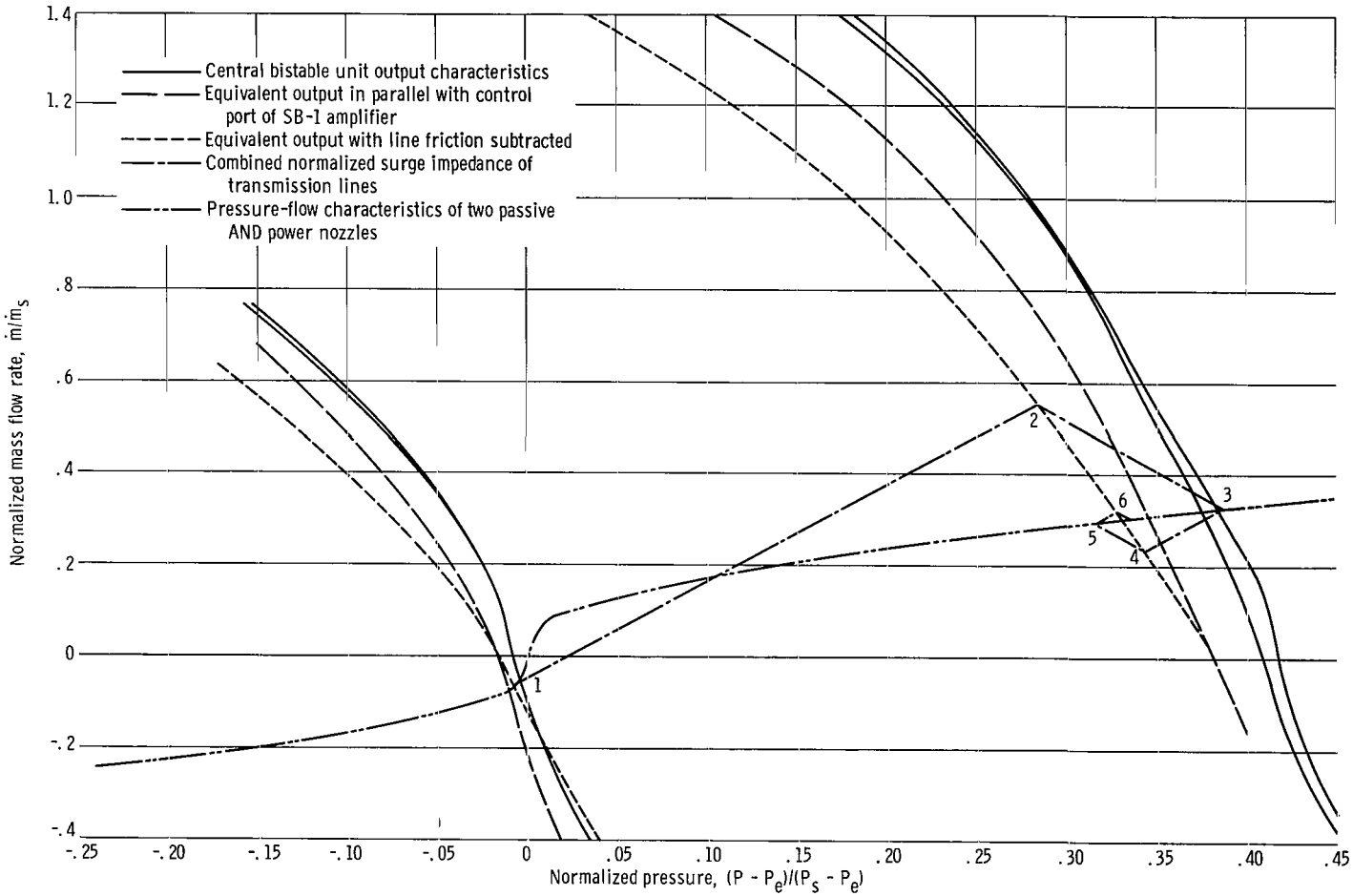

Figure 29. - Trajectory of carry signal.

APPENDIX C

DESIGN OF THE PULSE CONDITIONING UNIT

This appendix illustrates the techniques used to size the delay line and input orifice of the pulse width fixation portion of the pulse conditioning unit (fig. 8 (p. 11)). Typical calculations and graphs are included. The approaches to be described should be valid for use with any fluid jet amplifiers whose switching characteristics are fast in comparison with the duration of the delivered output pulse.

Choice of the proper input-orifice and delay-line diameters is made difficult by cross flow between the control ports of the fluid jet amplifier. When one control port of a bistable fluid jet amplifier is pressurized, the pressure-flow characteristics of the opposite control port are changed. Thus, an input orifice can be sized to set amplifier 3 (switch it to receiver R_2) when control port C_2 is left open to atmosphere. A delay-line diameter can be calculated which will reset it (switch it to receiver R_1) when control port C_1 is vented. However, because of control-port crossflow, the orifice and delay line, in combination, probably will not provide the signal to reset amplifier 3, once it has been set.

To account for the effects of control-port crossflow, it is necessary to obtain both a plot of the receiver output pressure-flow characteristics and a set of control-port pressure-flow characteristics as a function of opposite control-port pressure. The plots used are shown in figure 30 and were taken on the amplifier shown in figure 14(a) (p. 17). With the aid of these graphs, the following iterative procedure can be used to size both the input-orifice and delay-line diameters:

(1) An initial amplifier 2 output pressure is assumed. With this pressure, an input orifice is calculated which will furnish sufficient pressures and flows to set amplifier 3 (switch it to its receiver R_2).

(2) With the calculated input orifice and assumed amplifier 2 output pressure, an equivalent source for feeding control port C_1 may be constructed. By plotting the pressure-flow characteristics of this source on the control-port characteristics of amplifier 3 (figs. 30(a) and (b)), a set of values of $\left(P_{C_1} - P_e\right)/(P_s - P_e)$ as a function of $\left(P_{C_2} - P_e\right)/(P_s - P_e)$ may be determined.

(3) With the orifice calculated in step (1), an equivalent input-pressure-flow characteristic for the input orifice - control port C_1 combination may be constructed ($P_{C_2} - P_e$ is assumed to be zero). This pressure-flow characteristic is subtracted from the amplifier 2 output pressure-flow characteristic to give an equivalent source which is available for driving the delay line.

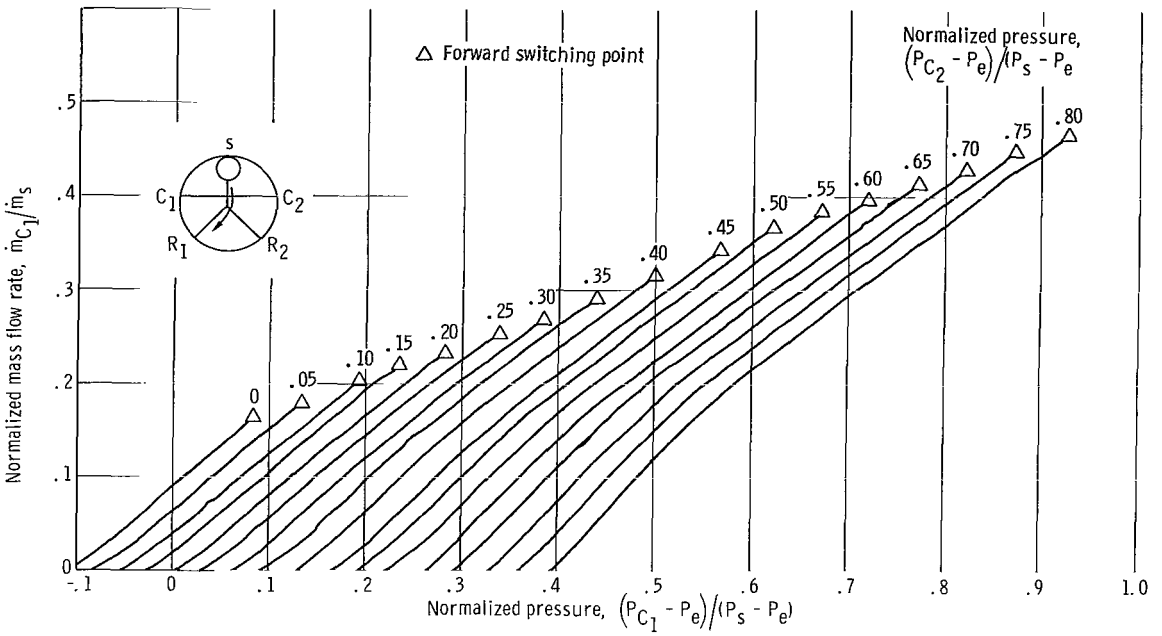

(a) Unswitched control port, amplifier 3; supply pressure minus exhaust pressure, 3.0 psig (2.07 N/cm^2 gage).

Figure 30. - Pressure-flow characteristics.

(4) Given $(P_{C_1} - P_e)/(P_s - P_e)$ as a function of $(P_{C_2} - P_e)/(P_s - P_e)$, figures 30(a) and (b) can be used to determine the pressure-flow characteristics of control port C_2 of amplifier 3.

(5) The pressure-flow characteristics of control port C_2 determined in (4) are then plotted on the equivalent output characteristic determined in (3). This plot shows whether or not amplifier 2 can deliver sufficient pressure to reset the amplifier 3.

(6) If amplifier 2 can deliver sufficient pressure to reset amplifier 3, then a normalized delay-line impedance can be selected. Starting from the intersection of the control port C_2 characteristics of amplifier 3 with the unswitched output characteristics of amplifier 2, the impedance will intersect the switched output characteristics of amplifier 2 at a pressure equal to that assumed when calculating the orifice diameter in step (1). The resultant waves and reflections are then calculated by use of the techniques of appendix B to see whether an acceptable reset signal is delivered to control port C_2. If

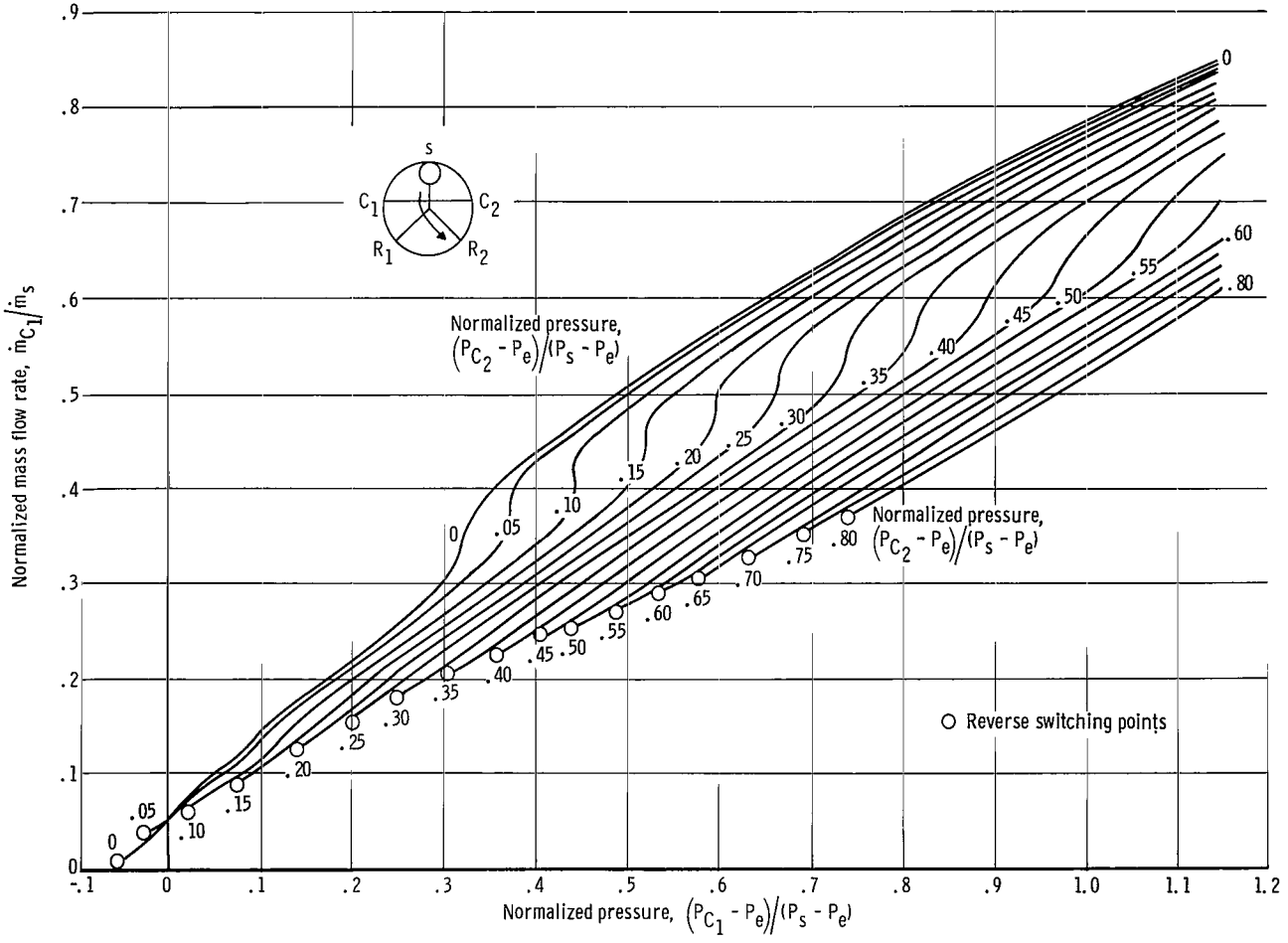

(b) Switched control port, amplifier 3; supply pressure minus exhaust pressure, 3.0 psig (2.07 N/cm^2 gage).

Figure 30. - Continued.

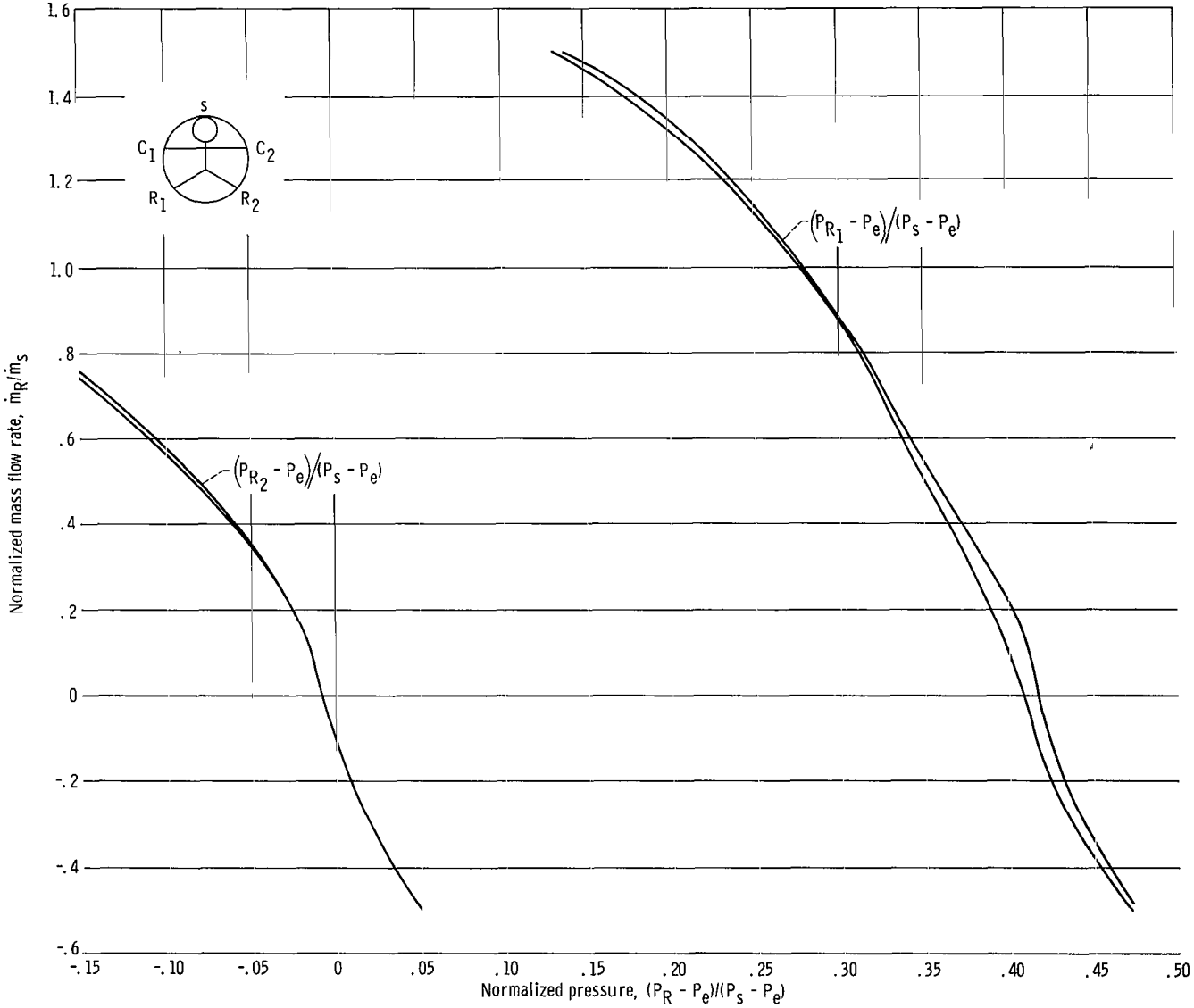

(c) Receiver, amplifier 2; supply pressure minus exhaust pressure, 6.0 psig (4.15 N/cm^2 gage).

Figure 30. - Concluded.

the signal delivered is satisfactory, a delay-line diameter is calculated directly, by use of equations (B2) or (B3). If the quality of the reset signal is not satisfactory, then a new output pressure from amplifier 2 is assumed, a new orifice diameter is calculated in (1), and the iteration procedure is repeated.

A typical iteration is given subsequently in illustration of the previously described procedure. The experimentally measured values of orifice diameter and timing pulse pressure are used in step (1) as initial values so that a comparison may be made between the predicted results and those actually obtained.

The supply pressures and power nozzle areas of amplifiers 1 to 3, were as follows:

$$P_s - P_e = 6.0 \text{ psig } (4.14 \text{ N/cm}^2 \text{ gage}) \text{ (supply to amplifier 2)}$$

$$P_s - P_e = 3.0 \text{ psig } (2.07 \text{ N/cm}^2 \text{ gage}) \text{ (supply to amplifier 3)}$$

$$(A_j)_{\text{amp 2}} = (A_j)_{\text{amp 3}} = 4.0 \times 10^{-4} \text{ in.}^2 \ (2.58 \times 10^{-3} \text{ cm}^2)$$

Since the power nozzle supply pressures, and hence flows, for the two amplifiers are different, scaling factors must be used when plotting the normalized characteristics of one on the normalized characteristics plot of the other. For these supply pressures, the corresponding pressure and flow scaling factors are:

$$\frac{(P_s - P_e)_{\text{amp 2}}}{(P_s - P_e)_{\text{amp 3}}} = 2.0$$

$$\frac{(\dot{m}_s)_{\text{amp 2}}}{(\dot{m}_s)_{\text{amp 3}}} = 1.415$$

Thus, if the control-port characteristics of amplifier 3 are to be plotted on the receiver characteristics of amplifier 2, its normalized pressures must be divided by a factor of two and its normalized flows by a factor of 1.415.

Step 1

An inlet orifice diameter of 0.0135 inch (0.343 mm) and an initial pulse height of 1.9 psig (1.31 N/cm^2 gage) are assumed to be the actual, final values. Plotting the

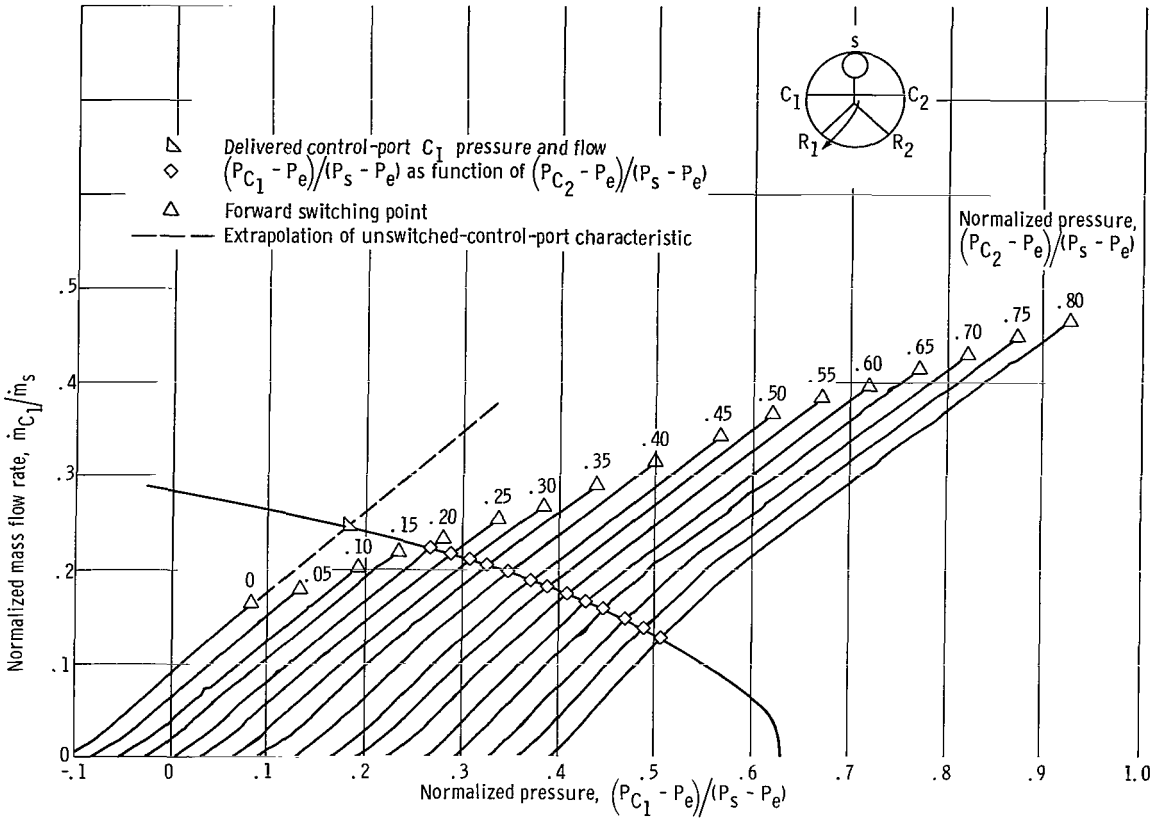

Figure 31. - Determination of initial pressures and flows delivered to control port C_1 of amplifier 3 and normalized pressure $(P_{C_1} - P_e)/(P_s - P_e)$ as function of normalized pressure $(P_{C_2} - P_e)/(P_s - P_e)$. Amplifier switched to control port C_1.

output pressure-flow characteristics of this source on the unswitched amplifier 3 control-port characteristics indicates that a switching, or set pressure, of 0.175 $(P_s - P_e)$ will be delivered to the control port (fig. 31). Since this pressure is higher than the actual switching pressure, the control-port characteristic is extrapolated past its triggering point and is shown as a dashed line.

Step 2

The orifice pressure-flow characteristic is also plotted on the switched control-port characteristic (fig. 32). The values that $(P_{C_1} - P_e)/(P_s - P_e)$ assumes for various values of $(P_{C_2} - P_e)/(P_s - P_e)$ is specified by the intersections of the constant $(P_{C_2} - P_e)/(P_s - P_e)$ lines with the orifice output pressure-flow characteristic. Fig-

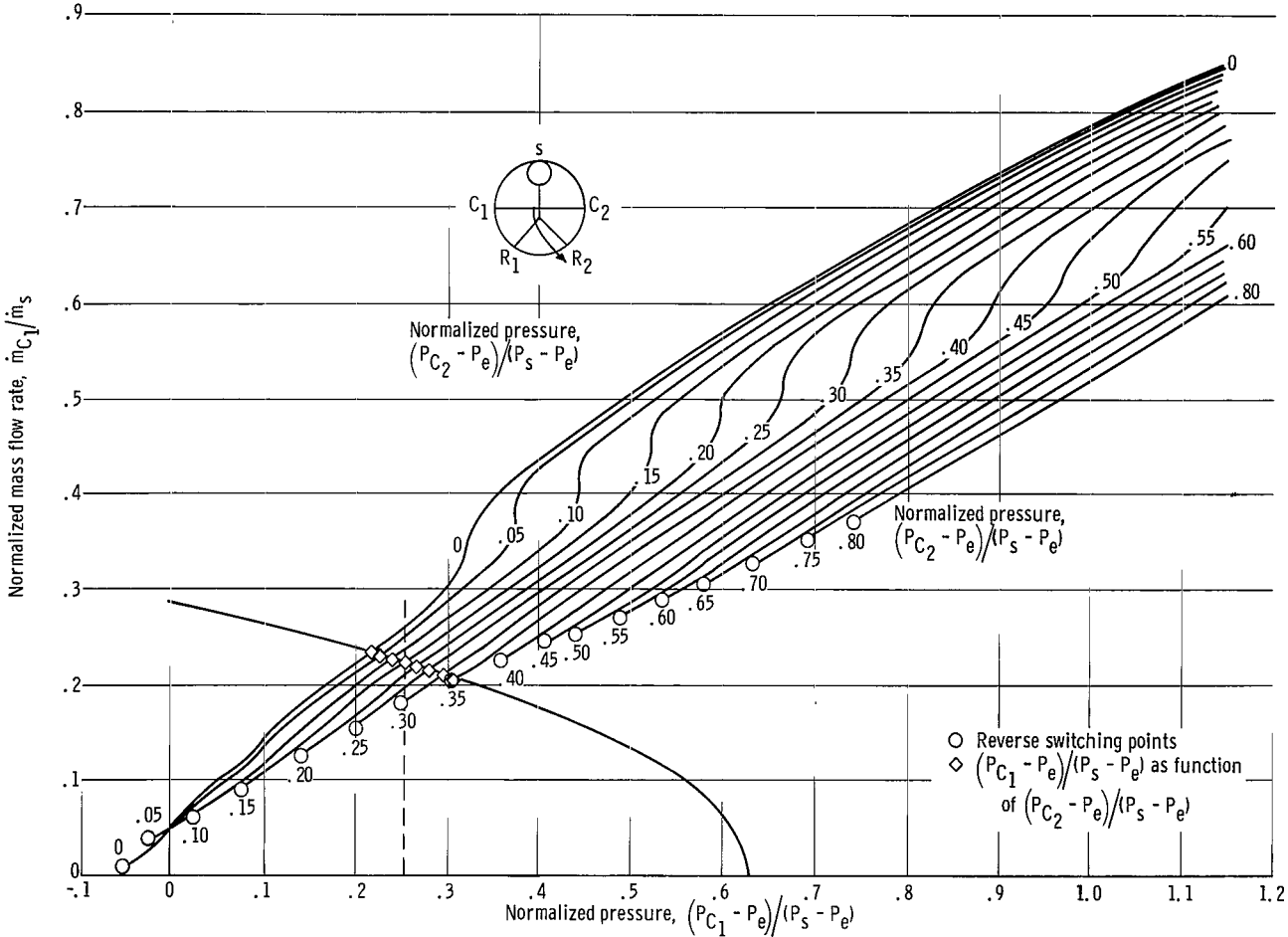

Figure 32. - Determination of values of normalized pressure $(P_{C_1} - P_e)/(P_s - P_e)$ as function of normalized pressure $(P_{C_2} - P_e)/(P_s - P_e)$. Amplifier 3 switched to control port C_2.

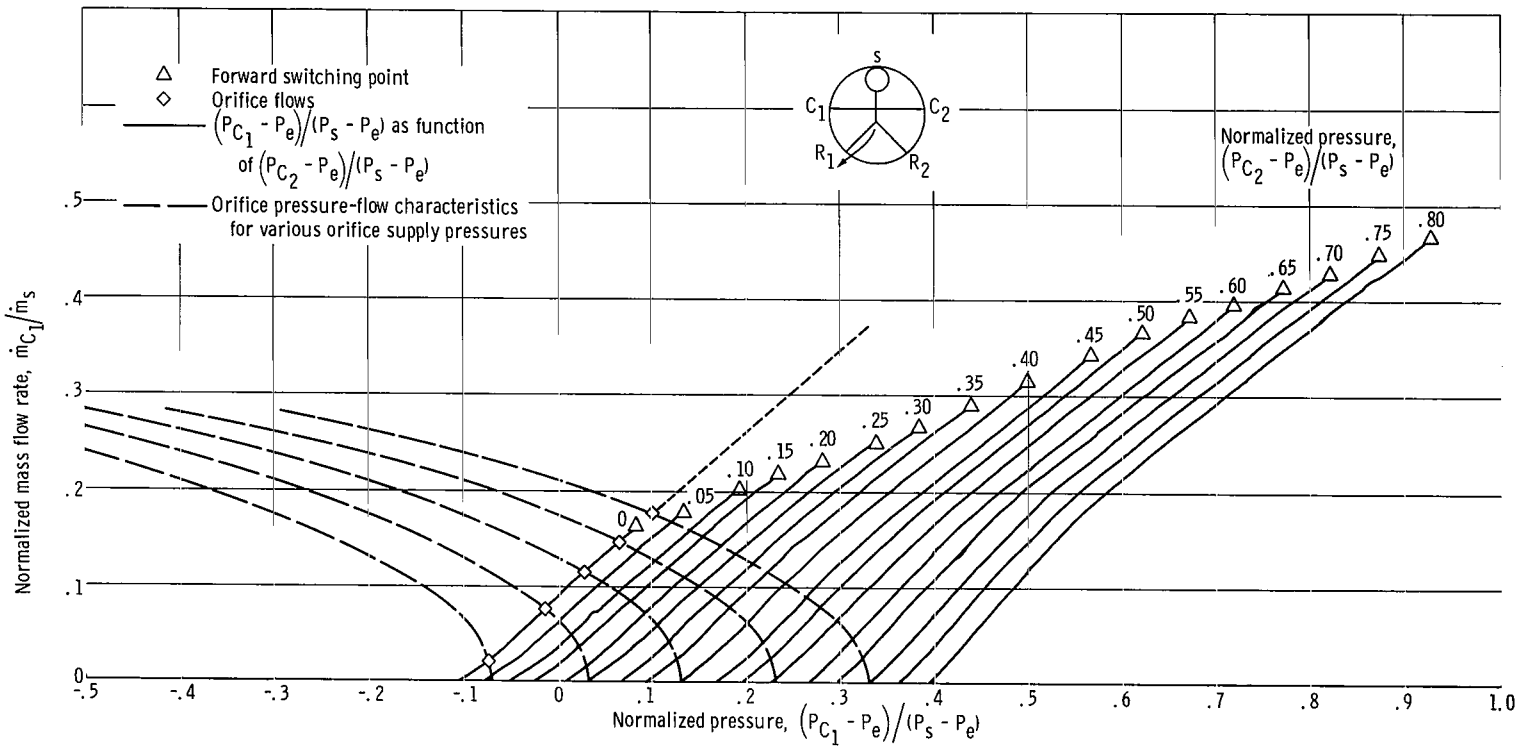

Figure 33. - Determination of feed orifice input pressure-flow characteristics. Amplifier 3 switched to control port C_1.

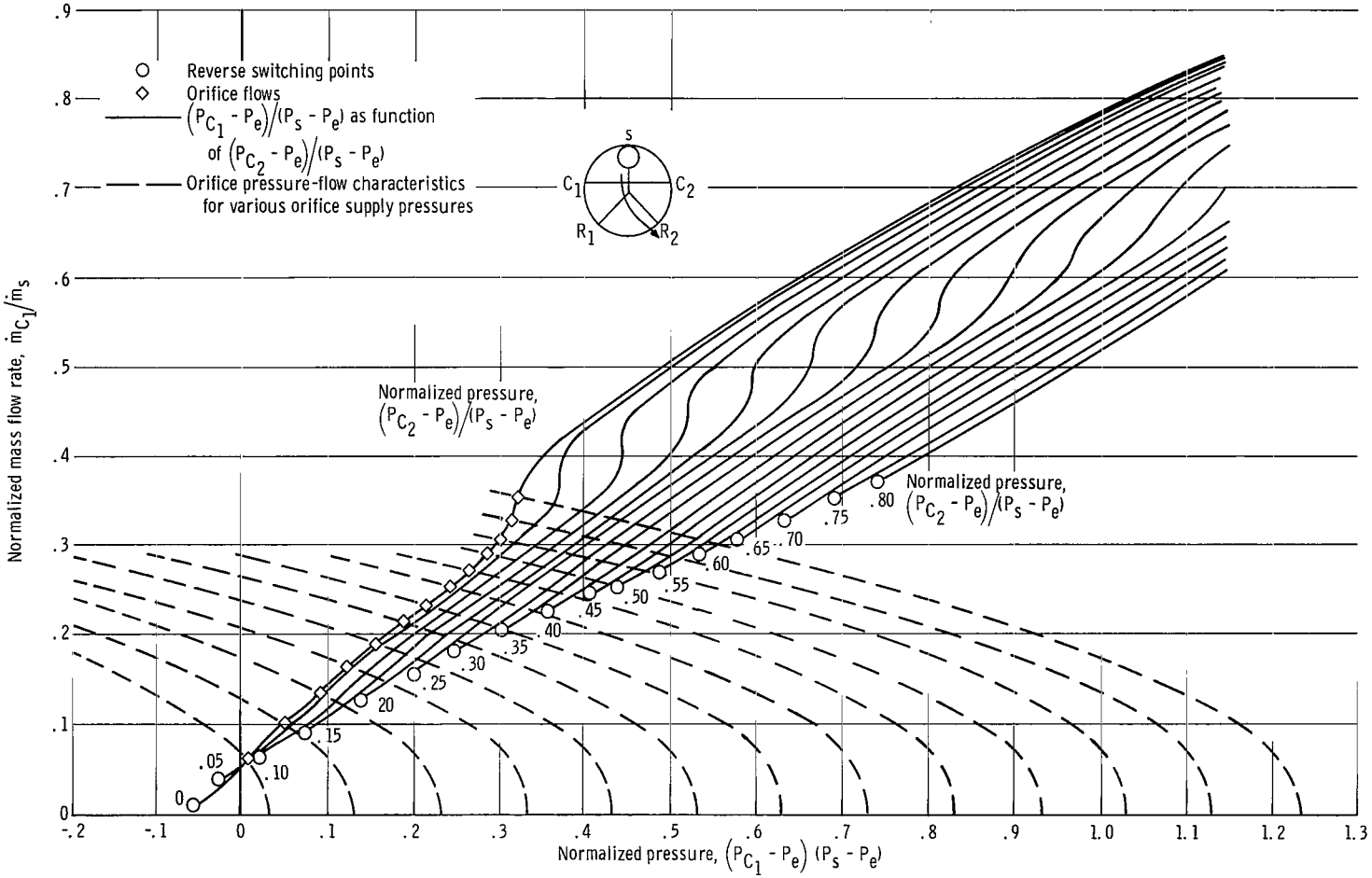

Figure 34. - Determination of orifice input pressure-flow characteristics. Amplifier 3 switched to control port C_2.

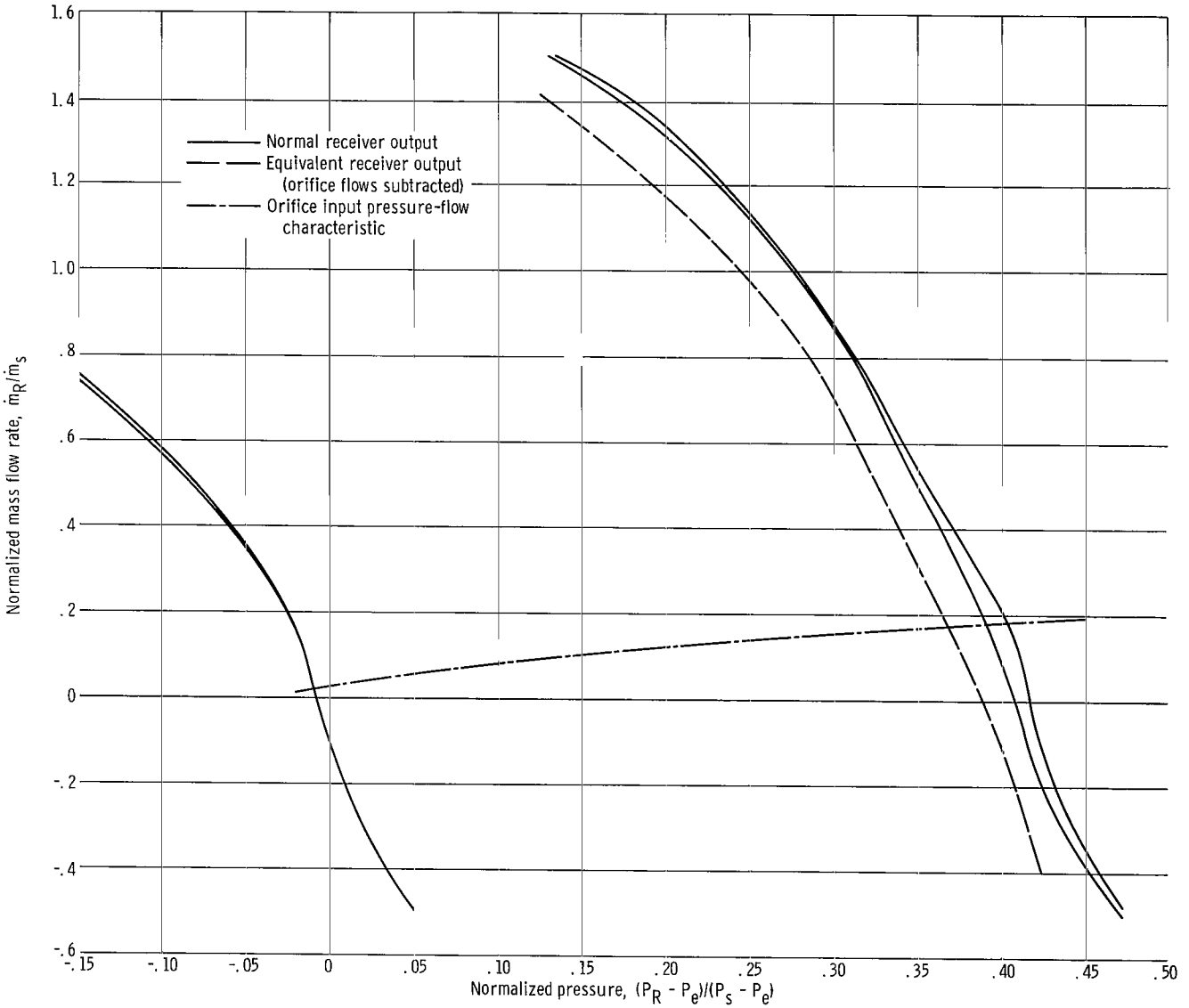

Figure 35. - Equivalent amplifier 2 receiver output characteristic.

ure 31 is used when the power jet is switched to receiver R_1, and figure 32 is used when the jet is directed toward receiver R_2. Thus, for example, figure 32 shows that a C_2 control-port pressure of $\left(P_{C_2} - P_e\right)/(P_s - P_e) = 0.15$ will cause the C_1 control-port pressure to rise to $\left(P_{C_1} - P_e\right)/(P_s - P_e) = 0.25$. This value is shown as a vertical dashed line in the figure.

Step 3

To determine the input pressure-flow characteristics, the source curve of the input orifice was shifted sideways on the two control-port characteristics plots. The intersection of the shifted orifice source curve with the horizontal (pressure) axis indicates the amplifier 2 pressure which is driving the orifice. The intersection of the orifice curve with the zero opposite control pressure curve $\left(P_{C_2} - P_e\right)/(P_s - P_e) = 0$ determines the flow which control port C_1, and hence the orifice, will consume. Shifting the orifice output curve sideways without changing its form may be justified on the basis that the flow through the orifice is approximately incompressible and the upstream density of the fluid does not change appreciably for the amplifier 2 output pressures that are encountered. The $\left(P_{C_2} - P_e\right)/(P_s - P_e) = 0$ line was used to determine control-port C_1 flows, since control-port C_1 flow consumption is of interest only to determine the pressures and flows available for driving the delay line. During the time when the initial portion of the delay-line pulse is being created, no pressures will be applied to control port C_2.

The resultant constructions are shown in figures 33 and 34. The intersections of the orifice output characteristics with the $\left(P_{C_2} - P_e\right)/(P_s - P_e) = 0$ line are shown as diamonds. The resultant pressure-flow curve determined by the intersections of the orifice curves with the horizontal pressure axis and the $\left(P_{C_2} - P_e\right)/(P_s - P_e) = 0$ line are plotted on the amplifier 2 receiver characteristics in figure 35. The equivalent amplifier 2 output characteristic when the orifice flows are subtracted from it is shown as a dashed line in figure 35.

Step 4

Because $\left(P_{C_1} - P_e\right)/(P_s - P_e)$ is uniquely related to $\left(P_{C_2} - P_e\right)/(P_s - P_e)$ as determined by steps 1 and 2, the control-port characteristic plots may be used again to determine the variation of $\dot{m}_{C_2}/\dot{m}_s$ as a function of $\left(P_{C_2} - P_e\right)/(P_s - P_e)$. Since the

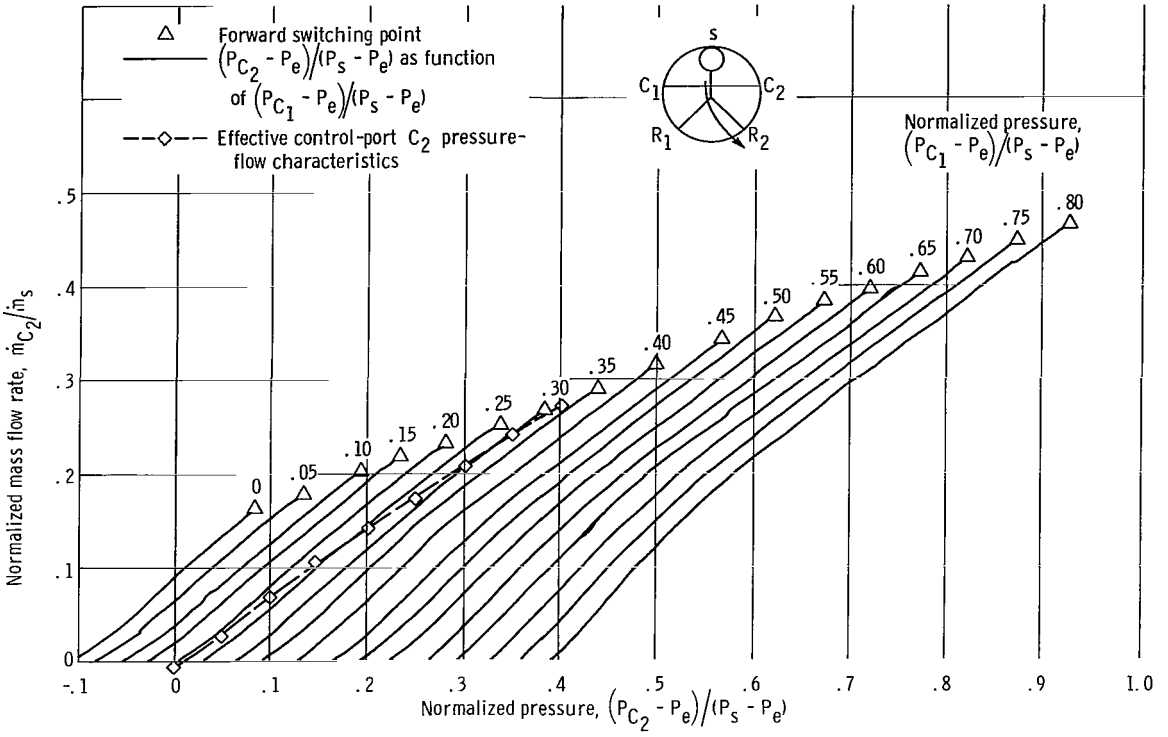

Figure 36. - Effective pressure-flow characteristics of control port C_2, amplifier 3. Amplifier switched to control port C_2.

amplifier is assumed to be symmetrical, the control-port characteristic plots shown in figures 31(a) and (b) can be used to represent control port C_2 as well as the control port C_1. The subscripts 1 and 2 on the plots are merely interchanged. By use of the orifice pressure-flow plots in figures 31 and 32, curves of $(P_{C_2} - P_e)/(P_s - P_e)$ as a function of $\dot{m}_{C_2}/\dot{m}_s$ may be obtained. These curves are shown in figures 36 and 37 as dashed lines. Figure 31 was used to obtain the curve in figure 37. Figure 32 was used to obtain the curve in figure 36. Values of $(P_{C_1} - P_e)/(P_s - P_e)$, as determined from step 2, for various values of $(P_{C_2} - P_e)/(P_s - P_e)$ are plotted as diamonds. The dashed line drawn through these points represents the effective input pressure-flow characteristics for control port C_2.

Step 5

The effective control-port C_2 characteristics determined in step 4 are multiplied by the previously determined scaling factors and plotted on the equivalent amplifer 2

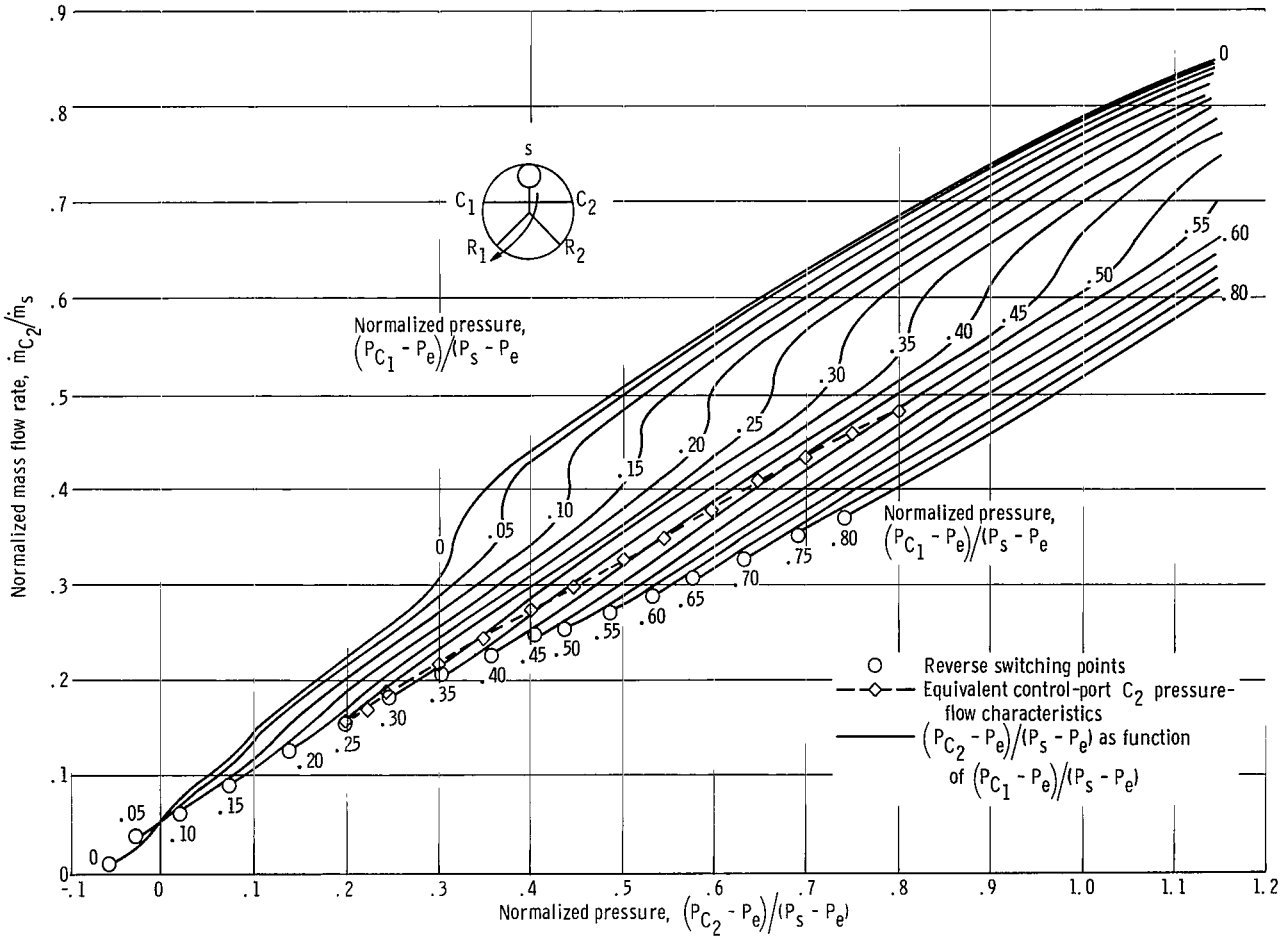

Figure 37. - Effective pressure-flow characteristics of control port C_2, amplifier 3. Amplifier switched to control port C_1.

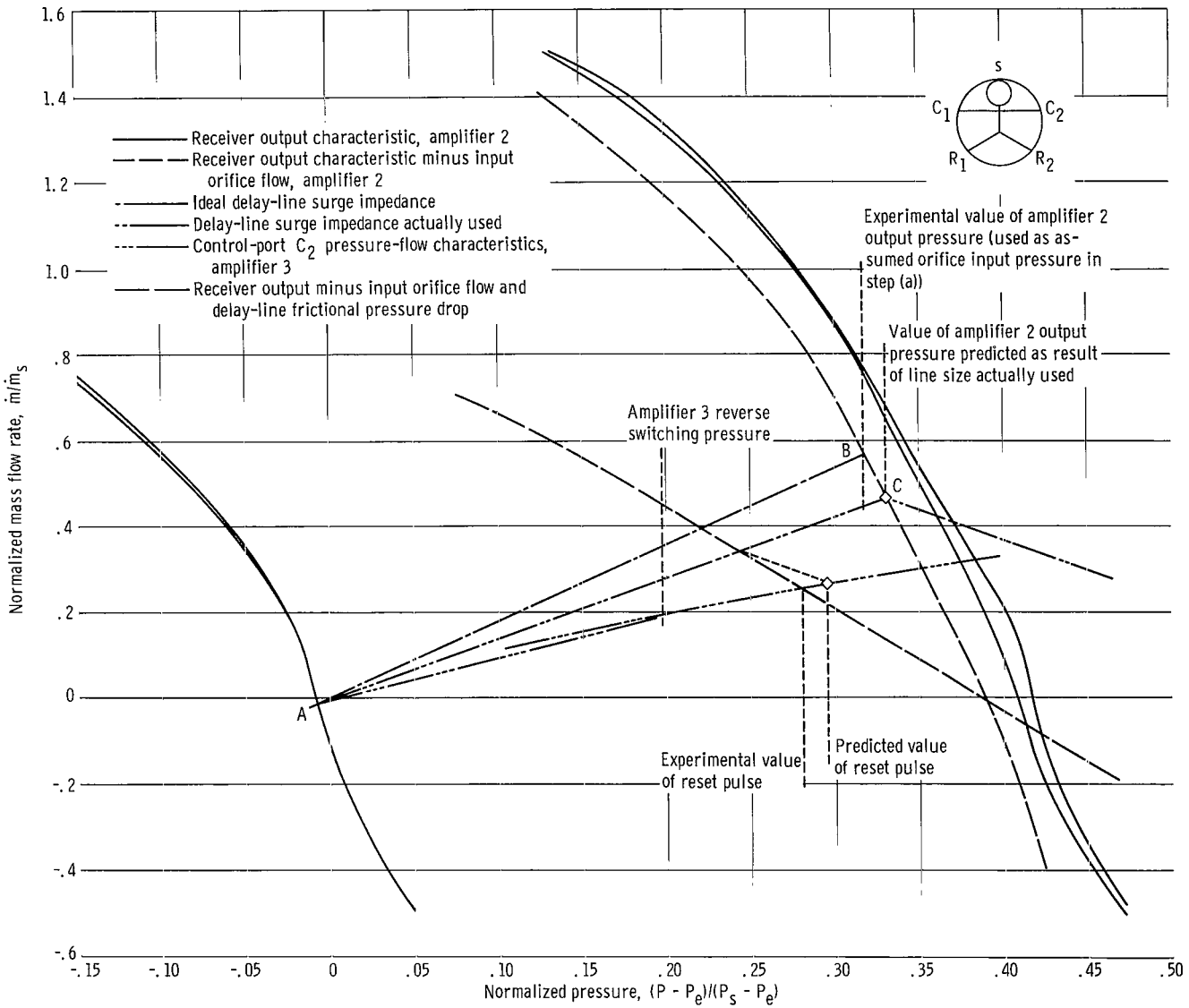

Figure 38. - Determination of value of reset pulse.

output characteristics. Thus, the dashed lines in figures 36 and 37 are scaled and plotted on the amplifier 2 output characteristics in figure 38.

As shown in figure 38, amplifier 2 can provide sufficient pressure and flow to reset amplifier 3. The delay-line surge impedance can be determined by drawing a line between point A, the initial condition of the delay line, to point B, the intersection of the initial assumed orifice pressure with the equivalent amplifier 2 output characteristic (shown as a short-dash line in fig. 38). The delay-line surge impedance cannot be arbitrarily chosen, as was done in appendix B. Its surge impedance is effectively specified by the initial pressures and flows in it before amplifier 2 is switched (point A) and the pressures and flows that result when amplifier 2 is switched into it (point B). These points were chosen at the beginning of the iteration procedure to size the input orifice. They must be used to calculate the delay-line impedance in order to maintain consistency in the calculations since both the delay line and the input orifice are driven in parallel by the same amplifier 2 receiver.

The line size corresponding to the impedance obtained by drawing a line between points A and B was not available and a slightly smaller one was used instead. Thus, as shown in figure 38, this smaller line should cause a slightly higher amplifier 2 output pressure to exist (point C) than was actually observed.

To compute the reset pulse delivered to control port C_2, the delay-line static pressure losses are first subtracted from the amplifier 2 output characteristics (as described in appendix B). The resultant equivalent output source is shown in figure 38. A small reflection occurs which is almost completely absorbed by the equivalent output source impedance. The predicted value of the reset pulse is close to the experimental and thus indicates the validity of the techniques used to size the delay line and to predict its performance. In particular, single reflection line termination was used to good advantage. A smaller line acoustically matched to the control-port C_2 impedance would have prohibitive frictional losses, and a pulse of insufficient magnitude to reset the amplifier would be delivered to the control port.

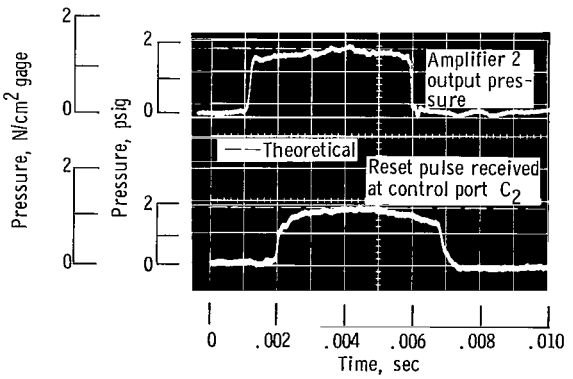

Figure 39. - Experimental traces of amplifier 2 output pressure and reset pulse delivered to control port C_2, amplifier 3.

Experimental pressure profiles of the pulse as delivered to the beginning of the delay line and as measured by a transducer approximately 1 inch (2.54 cm) from control port C_2 are shown in figure 39. The initial pulse rise time is fast and has a small step in it. This step, which is the reflected wave, appears since the transducer is a finite distance from the junction of the control port and the interaction region. If the transducer could have been mounted directly at the junction between the control port and the interaction region, this reflected wave would not have appeared as a separate pulse.

The lines between amplifiers 3 and 4 were sized for no-reflection termination by the procedures outlined in appendix B. The resultant output pulse delivered by amplifier 4 into an acoustically terminated 1/8-inch- (0.318-cm-) inside-diameter line is shown in figure 40. As is shown, a pulse with fast rise and decay times, constant amplitude, and 1-millisecond duration could be delivered by the pulse conditioning unit.

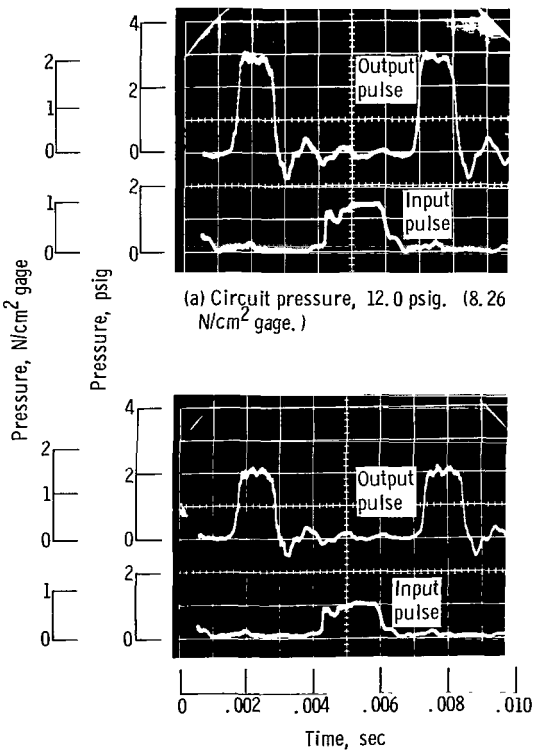

(a) Circuit pressure, 12.0 psig. (8.26 N/cm^2 gage.)

(b) Circuit pressure, 6.0 psig. (4.13 N/cm^2 gage.)

Figure 40. - Output of pulse conditioning unit.

APPENDIX D

SIMPLIFIED TRANSMISSION LINE

This appendix presents a brief treatment of an acoustically terminated pneumatic transmission line:

(1) To illustrate some of the effects resulting from transmission-line friction

(2) To provide justification for use of an equivalent source and frictionless transmission line to represent a transmission line with small but finite friction

Several sophisticated models of pneumatic transmission lines have been made which take into account the effects of time varient heat transfer and changing velocity profiles (refs. 7 to 9). Although the analyses accurately predict the performance of semi-infinite lines, they are hard to apply in a situation where numerous interactions can occur, by means of waves, between a nonlinear source and load. Thus, some authors have chosen to modify the simpler equations for an electromagnetic transmission line to represent the physically more complicated pneumatic line (refs. 10 to 12). If high accuracy is not desired and if appropriate corrections are made to account for changing velocity profiles and heat transfer, this latter approach can, on occasion, yield reasonable results (refs. 10 to 12). Because it can yield reasonable results with far less effort than the exact analysis, the electrical transmission-line analogy is used in this appendix to point out the effects of line friction.

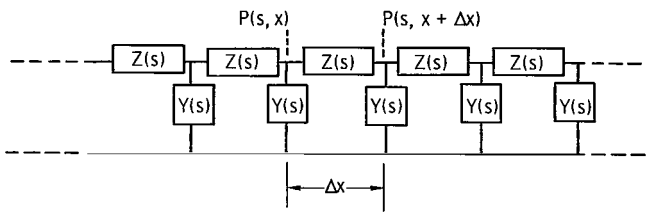

Figure 41. - Simplified model of transmission line.

Borrowing the analogy from electromagnetic transmission-line theory, the pneumatic transmission line may be regarded as composed of an infinite number of series impedances and shunt admittances, as shown in figure 41 (refs. 9, 11, and 13). The following equations for continuity and momentum can be written for an elemental length dx of the line (refs. 9, 11, and 13):

Continuity:

$$\frac{d}{dx}(\dot{m}(x, s)) = - Y(s)P(x, s) \tag{D1}$$

Momentum:

$$\frac{d}{dx}(P(x,s)) = -Z(s)\dot{m}(x,s) \tag{D2}$$

Combining equations (D1) and (D2) to solve for the pressure $P(x,s)$ and solving the resultant differential equation yield the following classical result for waves in a transmission line (refs. 9 and 14):

$$P(x,s) = P_A(s)e^{-x\Gamma(s)} + P_B(s)e^{x\Gamma(s)} \tag{D3}$$

where

$$\Gamma(s) = \sqrt{Z(s)Y(s)} = (s/C)\sqrt{\frac{\Re A_\ell g_o}{s}} \tag{D4}$$

is usually referred to as the propagation operator.

The mass flow $\dot{m}(s)$ may be solved for in terms of the initially applied pressure $P_a(s)$. From equation (D2)

$$\dot{m}(x,s) = -\frac{1}{Z(s)}\frac{d}{dx}\left[P(x,s)\right] = \frac{\Gamma(s)}{Z(s)}P_a(s)e^{-\Gamma x} - \frac{\Gamma(s)}{Z(s)}P_b(s)e^{\Gamma x} \tag{D5}$$

or

$$\dot{m}(x,s) = \frac{\Delta P(x,s)}{Z_c(s)} = \frac{P_a(x,s) - P_b(x,s)}{Z_c(s)} \tag{D6}$$

where

$$Z_c(s) = \sqrt{\frac{Z(s)}{Y(s)}} \tag{D7}$$

is usually referred to as the surge impedance of the line. For small friction and short times ($s \to \infty$), it can be assumed that

$$\frac{\Re A_\ell g_o}{s} \ll 1 \tag{D8}$$

which permits equations (D4) and (D7) to be rewritten

$$\Gamma x \cong \tau s + \alpha \tag{D9}$$

$$Z_c \cong Z_{co}\left(1 + \frac{\alpha}{\tau s}\right) \tag{D10}$$

where

$$\tau = \frac{x}{c}$$

$$\alpha = \frac{\Re x}{2Z_{co}}$$

If, for the moment, only right traveling waves ($P_b(s) = 0$) are considered,

$$P(x, s) \cong P_a(x)e^{-\tau s}e^{-\alpha} \tag{D11}$$

Thus, the term, $x\Gamma(s)$, consists of two terms, a pure delay and a pure attenuation.

Two features of the preceeding equations should be noted. The line acoustical impedance, after the wave has passed, continually increases with time, (the $\alpha/\tau s$ term). Thus, even though a step change in pressure is applied to one end of the semi-infinite line, it will accept less and less flow as time increases as a result of the increasing length of the line through which flow must travel in order to force the wave front of the pulse still further down the line.

The other unusual result is that pulse attenuation, for small values of α, is approximately equal to

$$\frac{P_a - P_x}{P_s - P_e} \cong \left(\frac{P_a - P_e}{P_s - P_e}\right)(1 - e^{-\alpha}) \cong \alpha\,\frac{(P_a - P_e)}{(P_s - P_e)} \cong \frac{\Re x}{2Z_{co}}\left(\frac{P_a - P_e}{P_s - P_e}\right) \frac{P_a - P_x}{P_a - P_e} \cong \frac{\Re x}{2Z_{co}} \tag{D12}$$

or approximately half the steady-state value that would occur if a resistive load equal to the line surge impedance Z_{co} were used to terminate the line at station X. Thus, it is evident that because of frictional effects a resistive load matched to the line characteristic impedance does not completely terminate the pulse.

Since a purely resistive load cannot completely absorb an incident pulse in a line which has friction, it is of interest to determine the approximate magnitude and duration of the readjustments in pressure which must occur at the end of the line. Stations at the

beginning and end of the line by the subscripts are denoted a and b, respectively, and the reflection coefficients of the source and load by

$$r_a(s) = \frac{Z_a(s) - Z_c(s)}{Z_a(s) + Z_c(s)} \tag{D13}$$

$$r_b(s) = \frac{Z_b(s) - Z_c(s)}{Z_b(s) + Z_c(s)} \tag{D14}$$

The Laplace transform of the pressure delivered to the terminating resistance may thus be expressed as

$$\left[P_b(s) - P_e\right] = \left[P_a(s) - P_e\right] \frac{Z_c(s)}{Z_c(s) + Z_a} \sum_{n=0}^{\infty} (r_a r_b)^n e^{-\Gamma l (2n+1)} (1 + r_b) \tag{D15}$$

where l is the length of the line. This derivation may be found in reference 13.

If the driving source is considered to be without output resistance (for convenience of analysis) the reflection coefficients may be rewritten

$$\left.\begin{aligned} r_a &= -1 \\ r_b &\cong -\frac{\alpha}{2\tau s} \end{aligned}\right\} \tag{D16}$$

For a step change in source pressure P_a, the Laplace transform of the delivered pressure pulse is

$$P_b(s) = \frac{P_a}{s} \sum_{n=0}^{\infty} \left(1 - \frac{\alpha}{2\tau s}\right)\left(\frac{\alpha}{2\tau s}\right)^n e^{-(2n+1)(\tau s + \alpha)} \tag{D17}$$

The inverse of this transform is the infinite series

$$P_a\left(\frac{t}{\tau}\right) = P_a \sum_{n=0}^{\infty} 1\left(\frac{t}{\tau} - m_n\right)\left(\frac{\alpha}{2}\right)^n \left(\frac{\frac{t}{\tau} - m_n}{n!}\right)^n \left\{ \left[1 - \frac{\left(\frac{\alpha}{2}\right)\left(\frac{t}{\tau} - m_n\right)}{n+1}\right] e^{-m_n \alpha} \right\} \tag{D18}$$

where

$$m_n = 2n + 1$$

and

$$\left.\begin{aligned} 1\left(\frac{t}{\tau} - m_n\right) &= 1.0 \quad \text{if} \left(\frac{t}{\tau} - m_n\right) \geq 0 \\ 1\left(\frac{t}{\tau} - m_n\right) &= 0 \quad \text{if} \left(\frac{t}{\tau} - m_n\right) < 0 \end{aligned}\right\} \tag{D19}$$

is the unit step function beginning at $t/\tau = m_n$.

An expansion of the first two terms of this series is shown in figure 42 for $\alpha = 0.1$. The transient has a form similar to an exponential decay and disappears by the time the reflected wave makes two traverses of the transmission line. Thus, for values of α equal to or less than 0.1 and pulse durations equal to or greater than 2τ, it would appear

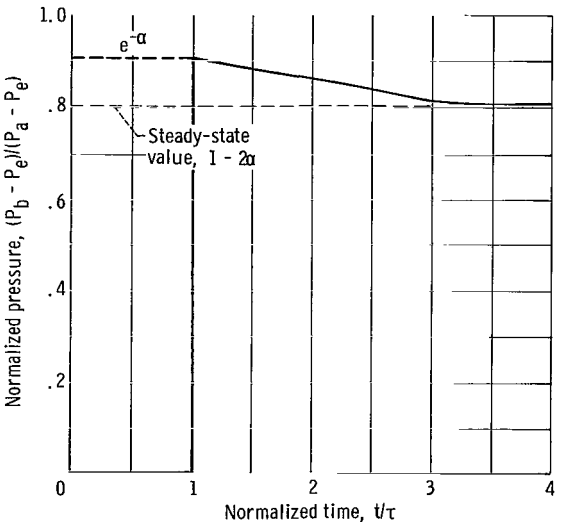

Figure 42. - Theoretical step response of resistively loaded transmission line with low internal friction. Attenuation term, α, 0.1.

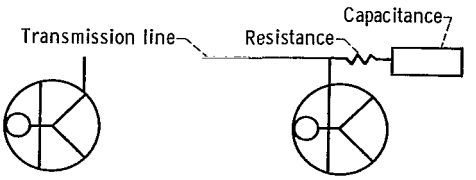

Figure 43. - Resistance-capacitance loading of transmission line to eliminate initial overshoot.

safe to neglect, entirely, the overshoot shown in figure 43. Also, the transient may be reduced by placing a resistance-capacitive (R-C) load in parallel with the purely resistive load which terminates the line (fig. 43). For pulse durations very short in comparison to 2τ, it would appear best to use only a resistive load and to compute the losses as being approximately α instead of 2α.

In summary, it would appear that the effects of small-line friction can be dealt with in the following approximate manner. For input pulses that are long in comparison with the transit time τ of the line, the transmission-line dynamics may be analyzed as if the line were frictionless but with a source which has the line steady-state pressure losses subtracted from it. The small transient appearing at the beginning of the pulse may, if desired, be attenuated by a simple R-C network in parallel with the load. For input pulses that are short in comparison to the transit time of the line, the approach would be to construct an equivalent source from which half the steady-state losses were subtracted and again treat the line as if it were frictionless.

Since this analysis is based on electrical transmission-line theory and only approximates conditions in a pneumatic transmission line, its results are not highly accurate. Pulse dispersion, which occurs in the real case, is not predicted by this analysis. For short lines, the constant RLC model underpredicts frictional losses (refs. 10 to 12). Thus its results should be used only to indicate whether or not a pneumatic transmission line has acceptable or unacceptable losses.

APPENDIX E

SCALING FACTORS FOR USE IN CROSSPLOTTING CONTROL-PORT AND RECEIVER PRESSURE-FLOW CHARACTERISTICS

This appendix presents some convenient formulae for calculating the ratios of the power nozzle flows in two fluid jet amplifiers of different size and supply pressures. These ratios are used as scaling factors in flow when crossplotting control-port and receiver pressure-flow data, such as is done in appendixes B and C.

When both nozzles are operating in the approximately incompressible flow region,

$$\frac{\dot{m}_{s_1}}{\dot{m}_{s_2}} = \frac{A_{j_1}}{A_{j_2}} \sqrt{\frac{P_{s_1} - P_e}{P_{s_2} - P_e}} \tag{E1}$$

When nozzle 1 operates as an incompressible nozzle and nozzle 2 is compressible and unchoked,

$$\frac{\dot{m}_{s_1}}{\dot{m}_{s_2}} = \left(\frac{A_{j_1}}{A_{j_2}}\right)\left(\frac{A_{j_2}}{A_2^*}\right)\left[\left(\frac{2}{k}\right)\left(\frac{P_e}{P_{s_2}}\right)\left(\frac{P_{s_1} - P_e}{P_{s_2}}\right)\right]^{1/2}\left[\left(\frac{k+1}{2}\right)^{(k+1)/(k-1)}\right]^{1/2} \tag{E2}$$

For air, k = 1.4, and equation (E2) reduces to

$$\frac{\dot{m}_{s_1}}{\dot{m}_{s_2}} = 2.07\left(\frac{A_{j_1}}{A_{j_2}}\right)\left(\frac{A}{A^*}\right)_2\left[\left(\frac{P_e}{P_{s_2}}\right)\left(\frac{P_{s_1} - P_e}{P_{s_2}}\right)\right]^{1/2} \tag{E2a}$$

When both power nozzles are compressible and unchoked,

$$\frac{\dot{m}_{s_1}}{\dot{m}_{s_2}} = \left(\frac{P_{s_1}}{P_{s_2}}\right)\left(\frac{A_{j_1}}{A_{j_2}}\right)\frac{\left(\frac{A}{A^*}\right)_2}{\left(\frac{A}{A^*}\right)_1} \tag{E3}$$

REFERENCES

1. Howland, G. R.: Pneumatic Nutator Actuator Motor. Rep. No. BPAD-863-16719R (NASA CR-54788), Bendix Corp., Oct. 17, 1965.

2. Blaiklock, P.; and Sidel, R.: Development of a Pneumatic Stepping Motor System. Summer Course Notes 2.73, Massachusetts Inst. Tech., Dept. of Mech. Eng., July 1966.

3. Griffin, W. S.; and Cooley, W. C.: Development of High Speed Flueric Logic Circuitry for a Novel Pneumatic Stepping Motor. ASME-HDL Symposium on Fluidics, Chicago, May 5, 1967, pp. 402-414.

4. Gromen, William E.: A Transition Map Method of Counter Synthesis. Rep. No. EDC 1-65-35 (NASA CR-61056), Case Inst. Tech., 1965.

5. Griffin, William S.: Design of a Fluid Jet Amplifier with Reduced Receiver-Interaction-Region Coupling. NASA TN D-3651, 1966.

6. Shapiro, Ascher H.: The Dynamics and Thermodynamics of Compressible Fluid Flow. Ronald Press Co., 1953.

7. Iberall, Arthur S.: Attenuation of Oscillatory Pressures in Instrument Lines. J. Res. Natl. Bur. Std., vol. 45, no. 1, July 1950, pp. 85-108.

8. Nichols, N. B.: The Linear Properties of Pneumatic Transmission Lines. ISA Trans., vol. 1, no. 1, Jan.-Mar. 1962, pp. 5-14.

9. Brown, Forbes T.: Pneumatic Pulse Transmission with Bistable-Jet-Relay Reception and Amplification. Sc. D. Thesis, Massachusetts Inst. Tech., May 1962.

10. Schuder, C. B.; and Binder, R. C.: The Response of Pneumatic Transmission Lines to Step Inputs. J. Basic Eng., vol. 81, no. 4, Dec. 1959, pp. 578-584.

11. Rohmann, C. P.; and Grogan, E. C.: On the Dynamics of Pneumatic Transmission Lines. Trans. ASME, vol. 79, no. 4, May 1957, pp. 853-874.

12. Reid, Karl N., Jr.: Static and Dynamic Interaction of a Fluid Jet and a Receiver-Diffuser. Sc. D. Thesis, Massachusetts Inst. Tech., Sept. 1964.

13. Fodor, György (F. Petik, trans.): Laplace Transforms in Engineering. Akadémiai Kiadó, Budapest, 1965.

14. Guillemin, Ernst A.: Communication Networks. Vol. II, John Wiley & Sons, Inc., 1935.

"The aeronautical and space activities of the United States shall be conducted so as to contribute . . . to the expansion of human knowledge of phenomena in the atmosphere and space. The Administration shall provide for the widest practicable and appropriate dissemination of information concerning its activities and the results thereof."

—NATIONAL AERONAUTICS AND SPACE ACT OF 1958

NASA SCIENTIFIC AND TECHNICAL PUBLICATIONS

TECHNICAL REPORTS: Scientific and technical information considered important, complete, and a lasting contribution to existing knowledge.

TECHNICAL NOTES: Information less broad in scope but nevertheless of importance as a contribution to existing knowledge.

TECHNICAL MEMORANDUMS: Information receiving limited distribution because of preliminary data, security classification, or other reasons.

CONTRACTOR REPORTS: Scientific and technical information generated under a NASA contract or grant and considered an important contribution to existing knowledge.

TECHNICAL TRANSLATIONS: Information published in a foreign language considered to merit NASA distribution in English.

SPECIAL PUBLICATIONS: Information derived from or of value to NASA activities. Publications include conference proceedings, monographs, data compilations, handbooks, sourcebooks, and special bibliographies.

TECHNOLOGY UTILIZATION PUBLICATIONS: Information on technology used by NASA that may be of particular interest in commercial and other non-aerospace applications. Publications include Tech Briefs, Technology Utilization Reports and Notes, and Technology Surveys.

Details on the availability of these publications may be obtained from:

SCIENTIFIC AND TECHNICAL INFORMATION DIVISION

NATIONAL AERONAUTICS AND SPACE ADMINISTRATION

Washington, D.C. 20546